الجمهورية الجزائرية الديمقراطية الشعبية
People's Democratic Republic of Algeria
وزارة التعليم العالي و البحث العلمي
Ministry Of Higher Education & Scientific Research
جامعة الوادي
University of Eloued
كلية التكنولوجيا
Faculty of Technology
قسم الهندسة الكهربائية
Department of Electrical Engineering

A thesis submitted for the fulfillment of

the degree of

Master in Electrical Engineering

Option: Electrical Drive

Theme

Enhanced Control of a Photovoltaic Water Pumping System by DTC-SVM

Presented by

Hocine Ihab AZZA *and* ***Ahmed MESAI BELGACEM***

Board of Examiners:

Dr. Zohier TIR	Suprvisor	MCA
Dr. Youcef Bekkakra	President	MCA
Dr. Ismail Laib	Examiner	MCA

2019/2020

Dedication

I dedicate this thesis to my ***father****,*

I also dedicate it to my ***mother*** *who has taken the biggest part of sacrificing for our education. May* ***Allah*** *protect them.*

To my ***brothers*** *and* ***sisters****. To my* ***nephews*** *and* ***nieces****.*

To all my friends, in my life.

Hocine Ihab AZZA

Dedication

*I dedicate this thesis to my parent "**MESAI BELGACEM Elhadi**" and "**BEN ALI Teffaha**", who have taken the biggest part of sacrificing for my education. May Allah protect them.*

*To my brother: **Abdelbaki.***

*To my sisters: **Ikram** and **Sondos**.*

To all my friends, in my social and academic life.

Ahmed MESAI BELGACEM

Acknowledgments

First of all, I would like to thank God "Allah" the Most Gracious and the Most Merciful, for blessing me with knowledge and giving me strength, courage, patience, and serenity during all these years of study.

I would like to express my thanks to everyone that makes the achievement of this work. My great gratitude goes to my supervisors: ***Dr. Zohier Tir*** *for his continuous support, guidance, encouragement throughout my project, his extensive knowledge, and diligent working.*

I also wish to thank the President of the jury ***Dr. Bekkakra Youcef*** *and* ***Dr. Laib Ismail*** *for serving as my committee members and taking the time to revise my thesis. I am thankful that in the midst of all their activities, they accepted to be members of the reading committee.*

Last but not the least, I am grateful to my parents for their prayers, guidance, and support throughout my education. Their inspiration and encouragement have been invaluable.

تحسين التحكم في نظام ضخ المياه الكهروضوئي بناءً على تقنية التحكم المباشر في عزم الدوران مع تعديل طول النبضة الشعاعي (DTC-SVM)

ملخص - حاليا، العديد من الأماكن تعاني من مشـاكل في إمدادات المياه، مثل المواقع المعزولة في الصـحراء. كما يعد نظام ضـخ المياه بالطاقة الشـمسـية المسـتقل أحد الحلول المقترحة، والذي يحتاج إلى صيانة أقل مقارنة بأنظمة الطاقة الأخرى. حيث يتكون هذا النظام من مولد كهروضـوئي، متصـل بعاكس مصـدر جهد مزود بمحرك حثي مقترن بمضـخة ذات طرد مركزي. الهدف والغرض من هذه المذكرة هو اسـتخدام تقنية التحكم المباشـر في العزم (DTC) للتحكم في المحرك اللاتزامني الذي يستمد تغذيته عن طريق النظام الكهروضوئي، ولضمان التشـغيل الأمثل للطاقة لهذا النظام عند ظروف مناخية مختلفة بمعية تقنية التحكم DTC مع تعديل طول النبضـة الشعاعي (DTC-SVM) حيث يتم اسـتخدام خوارزمية P&O لإنشـاء المرجع المناسـب. نقدم بين يديكم هذا المحتوى والذي نناقش فيه النتائج المتحصـل عليها لهذا النظام وهذا للتحقق من أداءه وجودته ، وكل ذلك تم باستعمال برنامج ماتلاب للمحاكات.

الكلمات المفتاحية: المحرك اللاتزامني، التحكم المباشـر في العزم، مموج مصدر الجهد، تعديل الفضاء الشعاعي، الألواح الكهروضوئية، مضخة الطرد المركزي، الطاقة الشمسية ، (MPPT) تتبع النقطة القصوى للطاقة ، الطاقة المتجددة.

Enhanced Control of a Photovoltaic Water Pumping System by DTC-SVM

Abstract - This thesis proposes an improved provide a (DTC) technique to control the used motor in the photovoltaic system. The main contribution of this work ensures an optimum power operation (MPPT) of this system for different climate conditions, the (P&O) algorithm is used to generate the appropriate reference for direct torque control technique with space vector modulation (DTC-SVM). This is achieved by the stand-alone solar water pumping system is one of the proposed solutions for them, and it needs less intervention than other renewable energy systems by applying a system consists of a photovoltaic generator, which is connected to a voltage source inverter supplying an induction motor coupled to a centrifugal pump. To validate the whole system's performance, we presented and discussed the result using the MATLAB/SIMULINK software environment. The solar water pumping system is stable and gave satisfactory results, the DTC - SVM control is reduced the torque and flux ripples, with a fewer harmonics of induction motor current, where the electromagnetic torque of the induction motor tracked the load torque that was produced by the pump and controlled by DTC-SVM.

Keywords: Induction Motor, Direct Torque Control, Voltage Source Inverter, Space Vector Modulation, Photovoltaic, Centrifugal Pump, Solar Energy, Maximum Power Point Tracking.

List of figures

List of tables

List of Abbreviations

AC	Alternative Current.
DC	Direct Current.
DHI	Direct horizontal irradiance.
DNI	Diffuse normal irradiance.
DSC	Direct Self Control.
DTC	Direct Torque Control.
IM	Induction Motor.
MPPT	Maximum Power Point Tracking.
MRAS	Model Reference Adaptive System.
PI	Proportional-Integral.
P&O	Perturb and Observe.
PWM	Pulse Width Modulation.
PV	Photovoltaic.
SFOC	Stator Filed Oriented Control.
SHE	Selected Harmonic Elimination.
SPWM	Sinusoidal Pulse Width Modulation.
SVM	Space Vector Modulation.
SVPWM	Space Vector Pulse Width Modulation.
VSI	Voltage Source Inverter.

List of Symbols

$V_{s\alpha}\ V_{s\beta}$	α and β components of stator voltage.
$i_{s\alpha}\ i_{s\beta}$	α and β components of stator current.
$\psi_{s\alpha}\ \psi_{s\beta}$	α and β components of stator flux.
$\psi_{r\alpha}\ \psi_{r\beta}$	α and β components of rotor flux.
ψ_s, ψ_r	Stator flux, Rotor flux.
$R_s\ R_r$	Stator and rotor resistances respectively.
$L_s\ L_r$	Stator and rotor inductances respectively.
$T_e, \mathrm{T_L}$	Electromagnetic torque, Torque Load.
σ	Blondel's coefficient.
M_{sr}	Stator-rotor mutual inductance
p	Number of poles pairs.
ω_r	Rotor speed.
ω_s	Synchronous speed.
J	Inertia moment.
f	Coefficient of friction.
V_{dc}	Dc-bus voltage.
S_{ψ_s}, S_{T_e}	Flux logic output, Torque logic output.
h_{ψ_s}, h_{T_e}	Hysteresis band of stator flux and torque.
θ_s	Flux angle.
δ	Load angle between the stator and rotor flux vectors.
T_s	Sampling time.
$T_1\ T_2$	Reference voltages vectors corresponding durations.
$K_p\ K_i$	Proportional and integral gains.
$V_{sd}\ V_{sq}$	Direct and quadratic stator voltage components.
$V_{rd}\ V_{rq}$	Direct and quadratic rotor voltage components.
$T_\mathrm{p}, \mathrm{K_1}$	Load pump, Proportional constant of the pump.
T, S	Temperature, Insolation.
ω_{ref}	Reference speed.

Table of Contents

GENERAL INTRODUCTION

General Introduction

In recent years, energy production has been a major challenge, where the energy demand increases depend on the increase in population growth, and in the remote places have more demand than others, especially for extracting the water [1]. Most of the electric power production depends on non-renewable resources such as petroleum, coal, natural gas, and nuclear power sources. These sources pose a big danger and threat to the environment. On the other hand, the use of renewable energy such as the sun's insolation, wind, and geothermal heat to produce electrical energy does not pollute the environment and preserve it, which is the perfect way to provide water in isolated areas [2].

In this thesis, the objective of our study is the implementation of a solar photovoltaic water pumping system based on DTC-SVM control for an Induction motor connected with a centrifugal pump [3], this system absorbs and stores the water from the well into a tank.

The present work is structured as follows:

In the first chapter, we present a theoretical overview of the photovoltaic and pumping systems, where we present some methods and techniques that allow us to extract the available maximum power that can be produced taking into account the influences of the temperature and insolation variation on the efficiency of the PV systems.

In the second chapter, we present the modelling of the essential parts of the studied system starting from the Induction Motor (IM) to the Voltage Source Inverter (VSI) and ending with the theoretical overview of the Space Vector Pulse Width Modulation (SVPWM or SVM) [4].

In the third chapter, we present the Direct Torque Control (DTC) incorporated with the SVM technique for induction motor drive. Yet, an accurate flux estimator is used to estimate the non-measurable state variables [5], [6]. Finally, we close this chapter by implementing the SVM-DTC technique using Simulink/Matlab with the discussion of the obtained results.

In the last chapter, we implement numerically the whole studied system that followed by comments on the obtained results under different conditions.

CHAPTER I

State of the Art of Solar Photovoltaic Water Pumping System

I.1 Introduction

The most common problems that face the rural owners are the absence of water and electricity, and the difficulty to provide the fuel in some places, knowing that it causes pollution. These entire problems negatively affect the pumping needs of the local community and irrigation, but when we can provide electricity, we can also provide water. The use of solar energy to pump the water from the well is a good choice in exchange for traditional pumping systems that use electricity and fuel energy. The PV pumping system is environmentally friendly, has low-cost energy from a renewable source, and it does not need frequent maintenance or fuel, using a photovoltaic system that produces electrical energy to feed a motor equipped with an external water pump. This water pumping supply system can be used in remote, and society places. Therefore, the water supply system based on photovoltaic technology is very important in our lives, so we have to study and develop the PV pumping systems more than before. In this chapter, we will present a state of the art of that system, and explain many basics and some technologies and methods that can make us use this system perfectly.

I.2 Photovoltaic water pumping system

The most common problem in remote places and the most isolated communities that are far from waterways and electricity grid. To ensure the water supply anywhere, we have to use a stand-alone power supply, and photovoltaic solar energy is one of the most common of these energies. This combination is called "Photovoltaic Water Pumping System" as presented in Figure I.1. This system is the perfect way to fix the water supply's problems, by extracting and pumping the water from a well even in rural areas and places, and that is the system’s goal. The photovoltaic water pumping system can be used in many domains, including residential, farming (irrigation, breeding, and agriculture), water purification, or firefighting. It combines two principle parts that are the photovoltaic system and the pumping system.

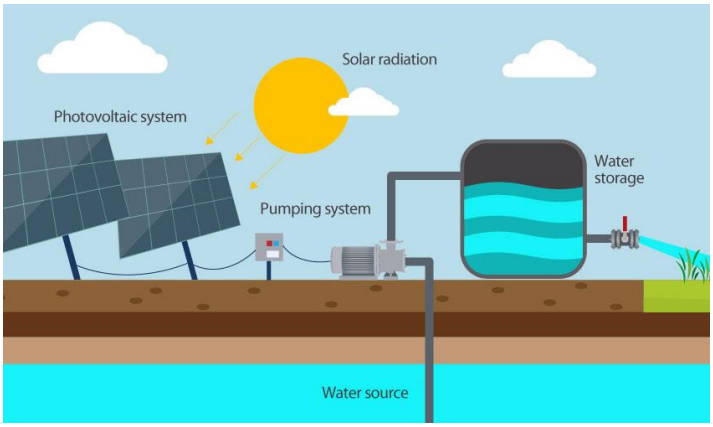

Figure I.1. *Photovoltaic Water Pumping System* [7].

I.3 Solar energy and photovoltaic system

I.3.1 Solar energy: why renewable energy?

Solar energy is a concept that refers to the radiation and heat of the sun exploited by various techniques of energy conversion, such as solar thermal collectors and photovoltaic cells, … etc. The biggest advantage of solar energy is that its source is stemming from the Sun which means is an endless source. Moreover, the sun shines every place on the earth that what makes it applicable to everyone. The other important advantages that these technologies present their lightness and viability for residential installation. Simply, everyone can install it, in his backyard or rooftop. Although the absence of solar irradiance is the most disadvantage that makes sometimes these technologies useless, also the solar energy may vary in its intensity from one place to another, which make its effectiveness is not the same on every place (effect of the temperature and the radiance), which will be discussed in the following sections of this chapter. Generally, we can divide the solar energy into two processes which are [8]:

1. Photovoltaic effect, which is the conversion of the sun's visible light into electricity.

2. Solar thermal, which is the transfer and the storage of the sun's heat for electricity heating purposes.

Our work is based on photovoltaic solar energy, which will explain in this chapter. Figure I.2 presents the difference between the two kinds of solar energy systems, which are the solar photovoltaic panel, and the solar thermal panel.

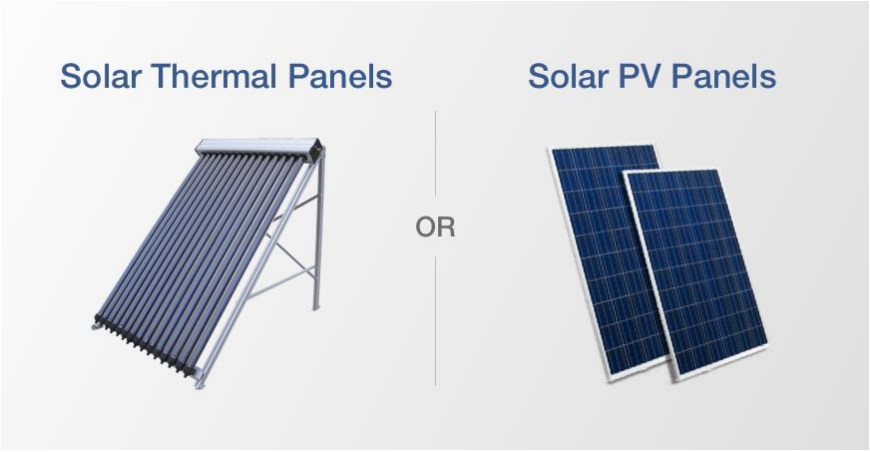

Figure I.2. *Solar Thermal Panel and Solar Photovoltaic Panel* [9]

I.3.2 Types of solar radiation

Solar radiation is classified into two types which are terrestrial radiation or extra-terrestrial radiation, depending on its location inside or outside the earth’s atmosphere respectively [8].

As shown in Figure I.3, the terrestrial radiation is also divided into two types: the first one is when the radiation comes from the sun directly and it is called direct normal irradiance (DNI), the second, the scattered radiation coming to the Earth's through the clouds, the ground or/and other objects surface known as diffuse horizontal irradiance (DHI), and some of them are re-scattered again by the atmosphere, they have also the same name diffuse horizontal irradiance (DHI). As well known, the Solar radiation is described as a flux of energy expressed in power per unit area (usual watts per square meters) [10], [11].

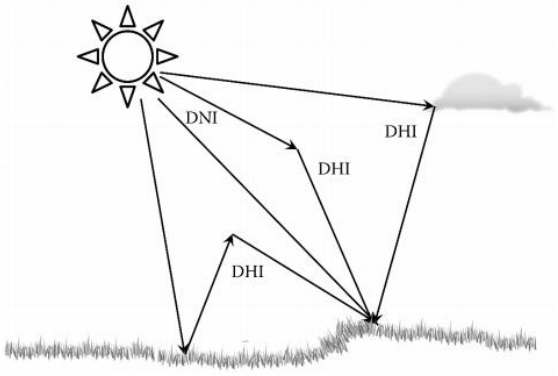

Figure I.3. *Solar radiation's components (DNI and DHI)* [10].

I.3.3 Photovoltaic solar energy

Photovoltaic solar energy is an innovative technique for transforming the most available solar energy to electrical energy without the use of internal combustion or rotating components [12]. That is happened using a solar panel based on the **photovoltaic effect,** it is defined by the hitting of the solar radiation on a photovoltaic cell that produces a direct current DC [13]. The absorption of solar radiation depends on the properties of the material of the solar cell [14]. The principal components of a photovoltaic system are solar cells (module, panel, and array) that receives the sun's radiation, and inverter, and electrical wires, and sometimes a storage battery [15].

I.3.3.1 Inverter

The inverter becomes a key device when the consumes requires the alternating currents AC, as well known, the principle of its work is to convert the energy provided by the PV systems as DC form to AC form [12].

I.3.4 Photovoltaic cells:

The photovoltaic solar cells are working as a generator of the electric current after receiving the solar radiation. The PV module is considered as PV cells in series. Also, the PV array is some

incorporated modules, which are connected in series or/and parallel. The series or/and parallel connection of the modules is related to the voltage or the current output that is needed by consumers. Figure I.4 shows the main components of the photovoltaic system [8].

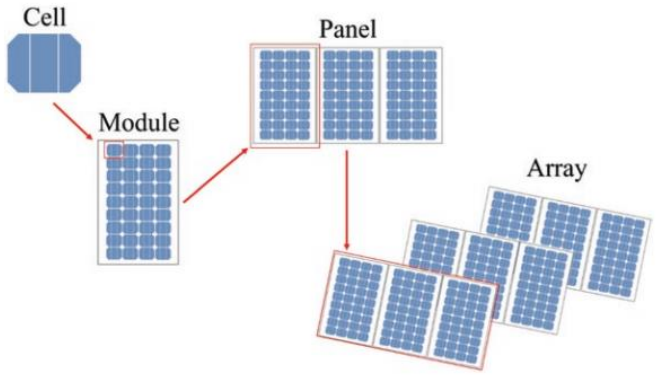

Figure I.4. *The main components of the photovoltaic system [8].*

There are many different types of photovoltaic cell technology, its association series or parallel, and its protection strategies. We will explain all that in the next paragraphs.

I.3.4.1 Type of PV cells technologies

The most common types of photovoltaic solar cells are the monocrystalline (single-crystalline), polycrystalline (multicrystalline), and noncrystalline (Amorphous) silicon cells [16]. Table I.1 presents the types of PV cells with their Efficiency and Expected lifetime.

Type of cell	Efficiency (%)	Expected lifetime (years)	References
Monocrystalline	17-22.7	25-30	International Energy Agency
Polycrystalline	10-14	20-25	Cotar and Flicik
Amorphous	6	15-20	Cotar and Flicik

Table I.1. *Types of PV cell with their Efficiency and Expected lifetime* [12].

- **The monocrystalline silicon cell** is produced by a homogeneous crystallinity, and it has high carrier mobility, high efficiency (17-22.7%), and high lifetime (25-30 years), but it is expensive compared with other types.
- **The polycrystalline silicon cell** has an irregular direction of its crystalline. Its photoelectric efficiency is lower than the single-crystalline silicon cell also it has a low cost compared to the monocrystalline cell.
- In terms of the **non-crystalline silicon cell,** it makes from non-crystalline silicon materials usually used to make thin-film solar cells. Non-crystalline silicon PV cell has low efficiency

but it is not expensive. They are usually used in weak light devices for example the cells of calculators.

According to the provided data in Table I.1, the optimum value of the efficiency and the lifetime refers to the monocrystalline silicon solar cells. Figure I.5 shows these three types of solar cells.

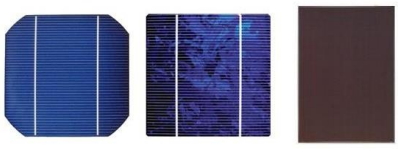

Figure I.5. *Types of the photovoltaic solar cell* [17].

I.3.4.2 Series, parallel and mixed combinations of PV modules

To provide the appropriate values of current and voltage, the solar modules must be properly connected between them to achieve the required value of current and/or voltage. So, there are two principals possibilities of the interconnection, which are the parallel or series combinations, and the mixing between them [8], [18].

- In the case of combinations of modules in series, the increase in voltage depends on the number of the series modules, in such case, the maximum power and current of the own modules are the same as shown in Figure I.6, when three solar modules are connected in series, where own solar module characterized by 6 volts and 3 Amps, in this case, the voltage and current of system output will be 18 volts and 3 Amps, respectively.

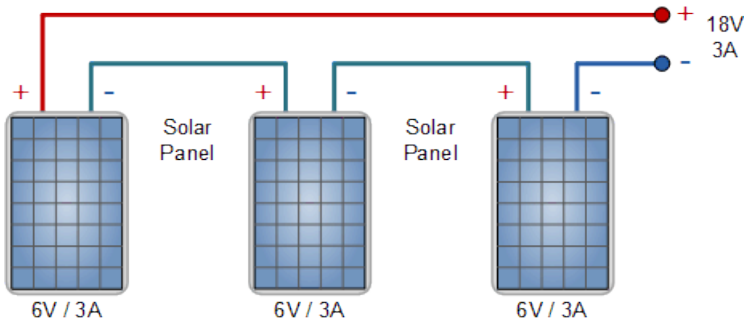

Figure I.6. *The serial connections of PV modules* [19].

- In the case of combinations of modules in parallel, the increase in current depends on the number of the parallel modules, in such case, the maximum power and voltage of the own modules are the same, as shown in Figure I.6, when three solar modules are connected in

parallel, where own solar module characterized by 6 volts and 3 Amps, in this case, the voltage and current of system output will be 6 volts and 9 Amps, respectively.

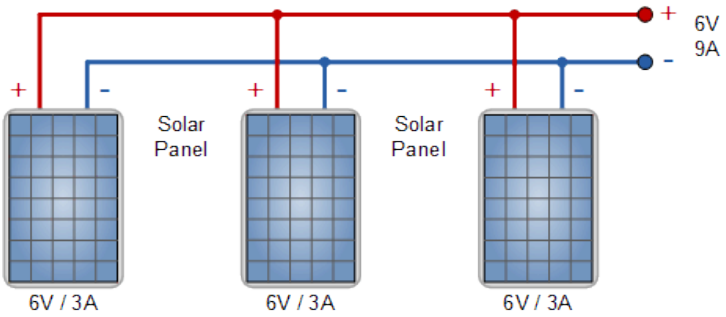

Figure I.7. *The parallel connections of PV modules* [19].

❖ A mixed combination allows us to increase the voltage and current at the same time.

I.3.4.3 Solar modules protection [20]

The solar modules are composed of many solar cells in which are connected in series, unfortunately, many risks can arise this PV module, this can damage it, perhaps like these risks: hotspot shaded cell or its connection with a battery without protections … etc. The Hotspot occurred when there is one low current cell in a string of at least several high short circuit current solar cells. This causes the shaded cell to produce a low current that flows through the good cells causing them to produce a higher voltage, which causes to be reverse biased and possibly increase local overheating.

I.3.4.3.1 Use of bypass diode

The key function of a bypass diode is to bypass the current from the shaded cell. For making the PV module still working even with the reduction in the output power. Generally, they use two bypass diodes for each module with 36 cells, and these bypass diodes can be combined in parallel with several cells. Figure I.8 shows the bypass diode role in the PV module.

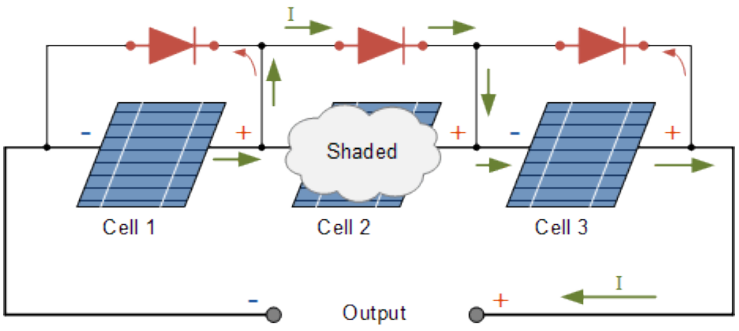

Figure I.8. *Shaded PV cells with Bypass Diodes protection* [19].

I.3.4.3.2 Use of blocking diodes

In night conditions where the solar radiations are missed; no voltage is generated by the solar panels, the battery's voltage producing a current which flows through the panels in the opposite direction. So to avoid this, blocking diodes are used to stop this problem as presented in Figure I.9.

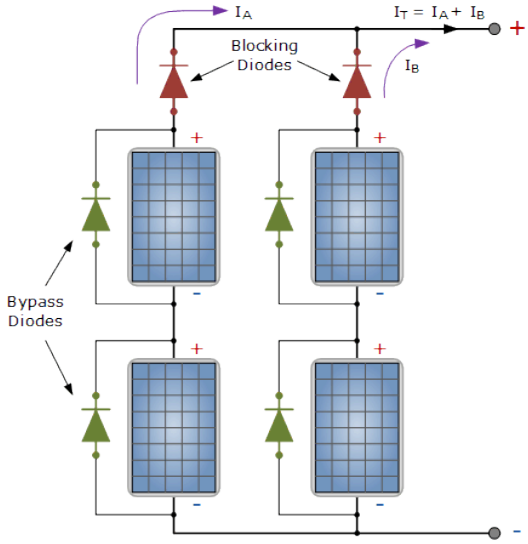

Figure I.9. *PV cells with Bypass and Blocking Diodes protection* [19].

I.3.5 Photovoltaic effect

The photovoltaic cell based on silicon consists of two thin layers of semiconductor, which are doped differently, see Figure I.10. where the sun's radiation fall on, the upper layer (2) is negatively doped with phosphorous, while the other lower layer (3) is positively doped with boron. Then, in the part between them, it knows as a p-n junction (1), where some electrical charges combine that where an opposite electrical field is created [12].

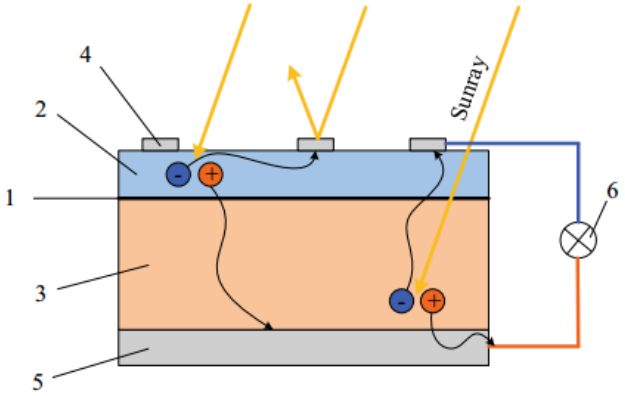

Figure I.10. *Component and operational principle of PV cells* [12].

where: (1) is p-n junction, (2) is the negatively doped layer, (3) is the positively doped layer, (4) is the negative electrode, (5) is the positive electrode, (6) is load.

I.3.6 Different types of PV systems

Solar PV systems are generally classified based on their operating requirements and the design of their connections. This PV Solar system can be classified as [8], [20], [21]:

I.3.6.1 Stand-Alone PV systems

A stand-alone PV installation is required in the off-grid PV system. This design is perfect for isolated and remote areas where electricity is required. Figure I.11 illustrates a standard stand-alone PV system.

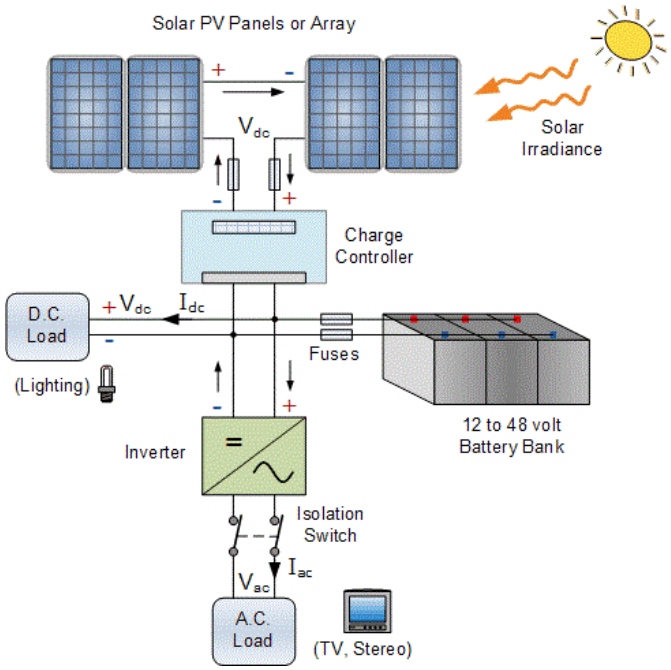

Figure I.11. *Standard Stand-Alone PV system* [19].

The PV system provides electricity from the sun's radiation. Therefore, they can only supply power during the day. That is why the battery banks are very important in this PV system type. Battery banks play a role of storing the generated power during the day, so that allows them to supply the consumers anytime.

I.3.6.2 Grid-Connected PV system:

As shown in Figure I.12, the well-known grid-connected PV system is usually composed of solar panels, charge controllers, battery banks, switchboards, smart inverter, and grid. This PV

system can be used either to fully supply the power to the network grid or to supply local load requirements.

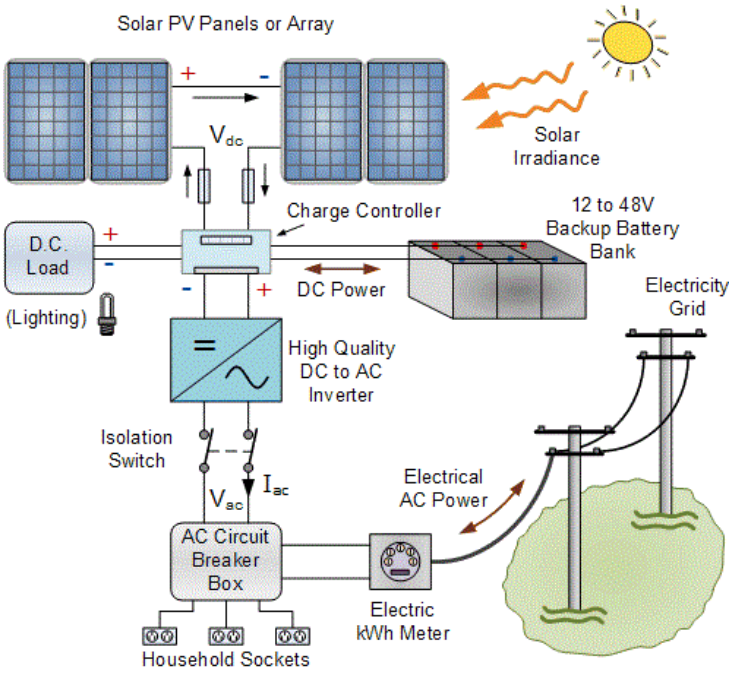

Figure I.12. *Standard Grid-Connected PV system* [19].

I.3.6.3 Hybrid PV system

As shown in Figure I.13, the hybrid systems usually refer to any two combines input sources or more, in which the PV solar may be combined with renewable or non-renewable energy sources. This type of system usually used a battery bank also for stocking the power coming from the PV system.

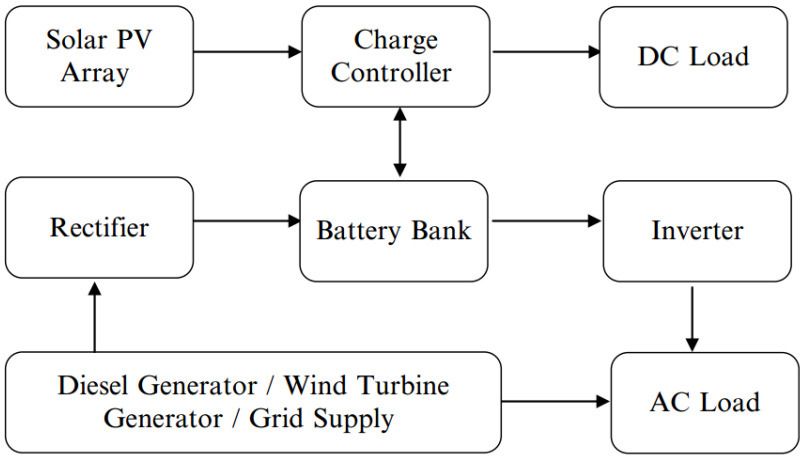

Figure I.13. *Standard Hybrid PV system* [21].

I.3.7 PV output characteristics and parameters

The PV cell's output is characterized using the current-voltage (I–V) and power–voltage (P–V) curves, these curves can represent the outputs of PV modules when their solar cells have uniform conditions. Figure I.14 shows typical I–V and P–V curves for a PV cell output [22].

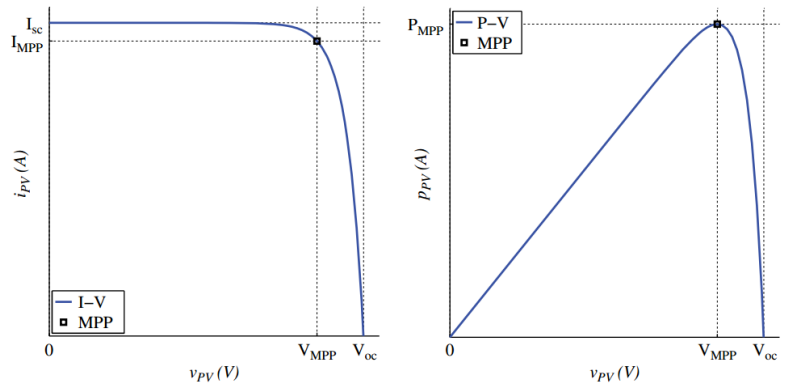

Figure I.14. *Typical I–V and P–V curves for a PV cell's output* [22].

I.3.8 Effect of solar irradiation and temperature [12]

I.3.8.1 Solar Irradiation effect

Throughout the day, solar irradiance has a higher variation more than the temperature, and it influences on the efficiency of the PV cells. As shown in Figure I.15, the electrical current generated depends directly on the absorbed solar radiation.

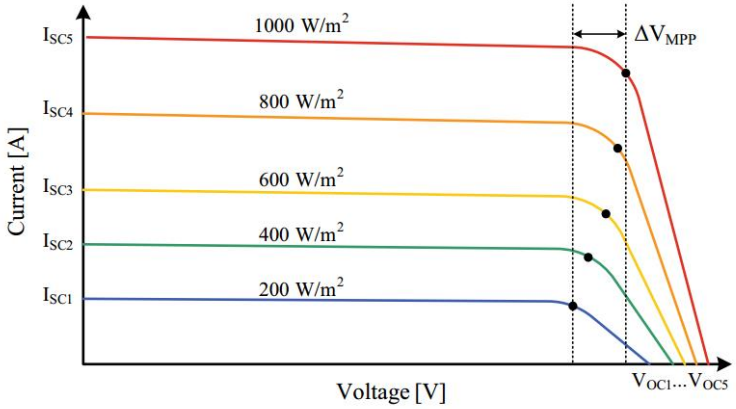

Figure I.15. *I–V Characteristic curve of a PV module* [12].

I.3.8.2 Temperature effect

As presented in Figure I.16, the voltage of the PV panel is influenced by the temperature variation. Using the same previous PV panel, the (V_{MPP}) value is less roughly during hot summer days by 10 V, and in the winter days is roughly higher than the STC (Standard Test Conditions) value by 10 V. However, the PV system current just barely increases with the temperature.

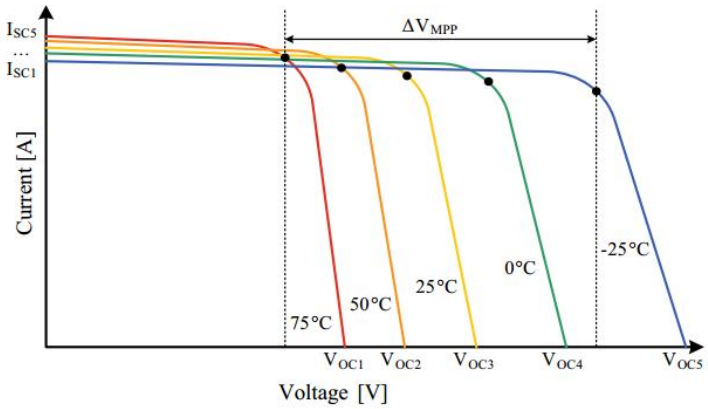

Figure I.16. *I–V Characteristic Curve of a PV Module at Constant Received Solar Radiation and Variable Temperature* [12].

I.3.9 Maximum Power Point Tracking control techniques

To exploit the majority of power that can be provided by the solar cell, a maximum power point of this can be tracked through a specific technique. The strategies of MPP tracking vary from one to other on many sides, like the range of performance, price, difficulty, used sensors, or their robustness control in specific conditions (variation in irradiation or temperature or both). The most common algorithms used for Maximum Power Point Tracking (MPPT) are "Hill Climbing/Perturb and Observe (P&O)" and "Incremental Conductance (InCond)", these two techniques are based on "Hill Climbing" concept, and this concept is based on the moving of the operation power point of the PV array to the increasing direction of the power [21].

I.3.9.1 Hill Climbing/Perturb and Observe

The operation of the P&O algorithm is based on the voltage and current sensors to provide an appropriate duty cycle to power converter according to the requirements of consumers. Also, such type of algorithm is known by its low cost computational. In this algorithm, the sign of the last disturbance and the sign of the last increment in the power is used to decide the next order. If the power value increase, the next perturbation should be kept in the same direction of the last one, else if the power value decrease, the next perturbation should be changed in the opposite direction of the last one. The cycle repeats until the MPP is satisfied.

Figure I.17 shows the orders of this process,

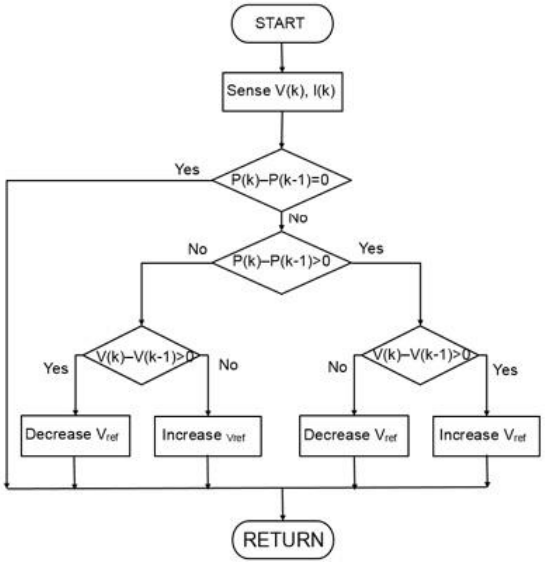

Figure I.17. *The cycle of the Perturb and Observe algorithm* [21].

I.4 Water Pumping System

It called also "Pump motors", they are widely used in irrigation systems, pools, and water pumping systems like pump water from groundwater sources.

These pumps comprise the following two principal components motor and pump, as their name indicates. The motor that produces the required pumping power and the pump uses the motor's power to pump the water from the well. The power source of our project is photovoltaic solar energy.

I.4.1 Motor technology

The most common types of motor that uses in Solar water pumps are:

- DC motors
- AC motors

The solar pump which uses an AC motor requires an inverter, in another case when the DC motor is needed, the boost-buck converter is required [23]. Generally, the AC motors are used in large scale systems in the contrary the DC motor is exploited in the small scale systems.

I.4.2 Pump technology

The most important component in the solar-powered pumping system is the pump. It can be divided into two categories; centrifugal and positive displacement pump. We will explain the centrifugal pump, which is included in our work.

I.4.2.1 Centrifugal pumps

As presented in Figure I.18, A centrifugal pump is a hydraulic mechanical system that works to flow up the water helping the rotational mechanical energy provided by motor drive, known as the impellers. This pump has one or multiple impellers that increase the water's pressure and velocity by spinning the water to subject it to centrifugal force, the water reaches to the rapidly rotating impeller and is directed to the pump's outlet by this force through the vane tips of the impeller along its circumference.

Figure I.18. *Surface Centrifugal Pump* [24].

To get a high-lift centrifugal pump, this pump must consist of several stages, each stage consisting of an impeller. Lifting capacity increases with the increasing each stage adds to the pump. Each stage adds pressure and friction, where the friction causes a decrease in the efficiency of each stage [24].

I.5 Conclusion

In this chapter, the description of the principal parts of the photovoltaic water pumping system is presented. Yet, the solar energy and photovoltaic system are well discussed, and the sun's radiation types are defined. Then, the most basics of the photovoltaic cells and their materials technology are presented also, the PV effect, and its different types system. Efficiency of the PV system are clarified depends on the solar radiations and temperature effects. To obtain the maximum power at the output of the pump system, the common type of MPPT algorithm named P&O is well explained in this chapter as well as its principle of operation. In the final of this chapter, the main components of the water pumping system are presented so as the type of the motors and pumps those can be used.

CHAPTER II

Induction Motor Modeling and Space Vector Modulation

II.1 Introduction

In this chapter, the induction motor modeling is described considering some assumptions, then, the Park transformation is exploited to make the motor easy to study. Therefore, a voltage source inverter is analyzed. Finally, both techniques of Pulse Width Modulation (PWM) and Space Vector Modulation (SVM) are also presented.

II.2 Description and mathematical model of induction motor

II.2.1 Description of the induction motor

The induction machines are usually used as motors for industrial applications due to their robustness and reliability. The induction motor has two main parts, one of them is **the stator** (a stationary part) and the second part is **the rotor** (a rotary part), the both parts are separated by an **air gap** between them [25]–[28].

The stator is containing three-phase winding in which may be connected in a star or delta connection. This three-phase winding is used to create a rotating magnetic field. As shown in Figure II.1, the stator is shown in *green* and the rotor in *blue* [29].

The rotor of the used induction motor is the type of squirrel-cage rotor as presented in Figure II.2 [30]. As known, almost 90% of induction motors that uses in industrials are squirrel cage motor due to its simple construction, its robustness, and its reliability in service.

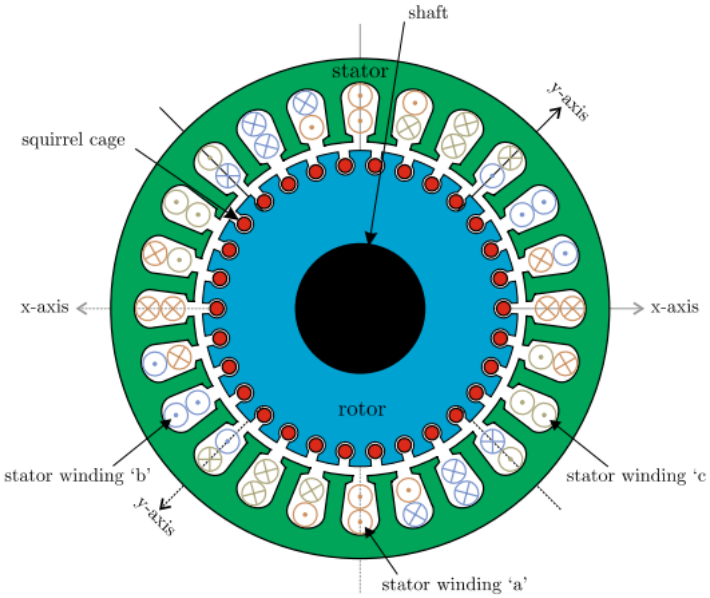

Figure II.1. *Cross-section of an Induction Machine* [31].

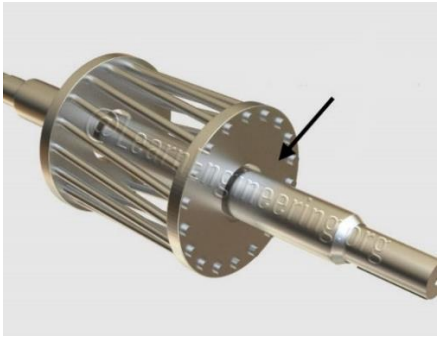

Figure II.2. *Squirrel-cage Rotors* [32].

II.2.2 Modeling assumptions

The model of the three-phase induction machine has been simplified by using these several hypotheses : [33]–[35]

- The MMFs created by the different circuits of stator and rotor are spread to have sinusoidal repartitions.
- The magnetic fields are supposed unsaturated.
- The skin effect does not exist.
- The machine has a constant air gap, which made the slotting effect is not taken account.

These hypotheses will make the modeling of the induction machine less complex, which allows developing the control methods easily.

II.2.3 Equivalent representation and vector formulation

As presented in Figure II.3, the induction machine is described by three symmetrical windings for each of the stator and the rotor phases whose axes are equitably distant between themselves by an electrical angle equal to 2π/3. Also, the three-rotor windings rotating at the mechanical speed (ω_r).

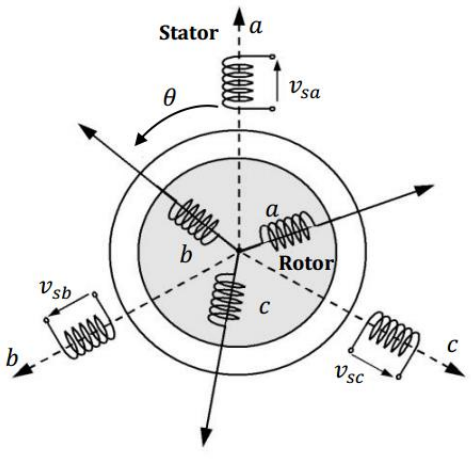

Figure II.3. *Induction Motor equivalent structure* [6].

By applying the Kirchhoff's laws on both circuits of the stator and the rotor, one can get :

II.2.3.1 Voltage equations

$$[v_{sabc}] = [R_s][i_{sabc}] + \frac{d}{dt}[\psi_{sabc}] \quad (II.1)$$

$$[v_{rabc}] = 0 = [R_r][i_{rabc}] + \frac{d}{dt}[\psi_{rabc}] \quad (II.2)$$

II.2.3.2 Flux equations

$$[\psi_{sabc}] = [L_s][i_{sabc}] + [M_{sr}][i_{rabc}] \quad (II.3)$$

$$[\psi_{rabc}] = [L_r][i_{rabc}] + [M_{sr}]^T[i_{sabc}] \quad (II.4)$$

where:

$$[v_{sabc}] = \begin{bmatrix} v_{sa} \\ v_{sb} \\ v_{sc} \end{bmatrix} ; [i_{sabc}] = \begin{bmatrix} i_{sa} \\ i_{sb} \\ i_{sc} \end{bmatrix} ; [\psi_{sabc}] = \begin{bmatrix} \psi_{sa} \\ \psi_{sb} \\ \psi_{sc} \end{bmatrix} \quad (II.5)$$

$$[v_{rabc}] = \begin{bmatrix} v_{ra} \\ v_{rb} \\ v_{rc} \end{bmatrix} ; [i_{rabc}] = \begin{bmatrix} i_{ra} \\ i_{rb} \\ i_{rc} \end{bmatrix} ; [\psi_{sabc}] = \begin{bmatrix} \psi_{ra} \\ \psi_{rb} \\ \psi_{rc} \end{bmatrix} \quad (II.6)$$

The subscripts s and r refer to the stator and the rotor, respectively, and the indices a, b, and c refers to the three phases. All resistances and inductances matrices are symmetric as seen below:

$$[R_s] = \begin{bmatrix} R_s & 0 & 0 \\ 0 & R_s & 0 \\ 0 & 0 & R_s \end{bmatrix} ; [R_r] = \begin{bmatrix} R_r & 0 & 0 \\ 0 & R_r & 0 \\ 0 & 0 & R_r \end{bmatrix} \quad (II.7)$$

$$[L_s] = \begin{bmatrix} L_s & M_s & M_s \\ M_s & L_s & M_s \\ M_s & M_s & L_s \end{bmatrix} ; [L_r] = \begin{bmatrix} L_r & M_r & M_r \\ M_r & L_r & M_r \\ M_r & M_r & L_r \end{bmatrix} \quad (II.8)$$

R_s and R_r, L_s and L_r are the resistances and self-inductances of the stator and the rotor, respectively.

M_S and M_r are the mutual inductance between two stator and rotor phases.

The mutual inductance between the stator and the rotor is considered as sinusoidal functions of the rotor position θ as following:

$$[M_{sr}] = [M_{rs}]^T = M_{sr}\begin{bmatrix} cos(\theta) & cos(\theta + \frac{2\pi}{3}) & cos(\theta + \frac{4\pi}{3}) \\ cos(\theta + \frac{4\pi}{3}) & cos(\theta) & cos(\theta + \frac{2\pi}{3}) \\ cos(\theta + \frac{2\pi}{3}) & cos(\theta + \frac{4\pi}{3}) & cos(\theta) \end{bmatrix} \quad (II.9)$$

M_{sr} is the maximal mutual inductance between the stator and the rotor phases.

II.2.3.3 Mechanical equations

The mechanical equation of IM is described as :

$$J\frac{d\omega_r}{dt} = T_e - T_L - f\omega_r \quad \text{(II.10)}$$

ω_r, T_e and T_L are the rotor speed, the electromagnetic torque, and the load torque respectively.

J is the inertia moment,

f is the friction coefficient.

II.2.4 Park transformation

To simplify the control and the study of an AC machine, one of the uses is Park transformations by which the three-phase stationary frame (a, b, c) can be transformed into the two-phase direct-quadrature frame (d, q) [6], [36]. The Park transformation's representation, in general, is given as:

$$\begin{bmatrix} x_d \\ x_q \\ x_0 \end{bmatrix} = P(\theta)\begin{bmatrix} x_a \\ x_b \\ x_c \end{bmatrix} \quad \text{(II.11)}$$

$$P(\theta) = n\begin{bmatrix} cos(\theta) & cos(\theta - \frac{2\pi}{3}) & cos(\theta - \frac{4\pi}{3}) \\ sin(\theta) & sin(\theta - \frac{2\pi}{3}) & sin(\theta - \frac{4\pi}{3}) \\ 1/2 & 1/2 & 1/2 \end{bmatrix} \quad \text{(II.12)}$$

Where θ is the angle between the axis-a and the axis-d, k is defined as a constant.

Figure II.4 has illustrated the passage of a three-phase stationary system (a,b,c) to the equivalent two-phase fixed system (α, β) then to the rotating frame (d, q).

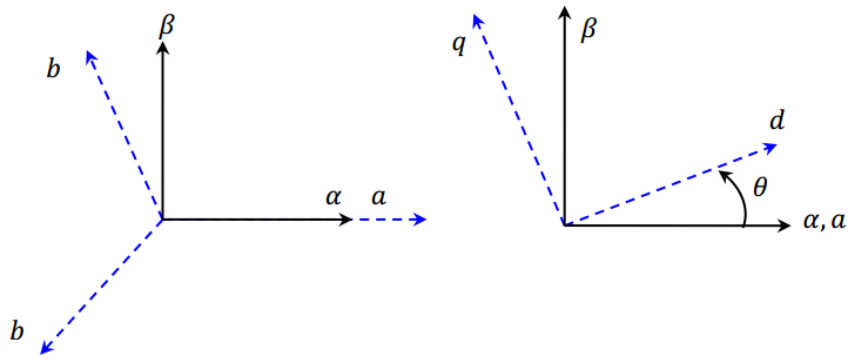

Figure II.4. *The passage of three-phase to a two-phase system using PARK transformation* [6].

II.2.5 Two-phase models of induction machine

one can simplify the three-phase model of the IM by applying Park transformation, where all their equations are rewritten in the two-phase rotating frame (d, q).

II.2.5.1 Voltage and flux equations in (d, q) frame

After applying the Park transformation on the equations of the induction machine (II.1-II.4) get the following (d, q) equations:

$$\begin{bmatrix} v_{sd} \\ v_{sq} \end{bmatrix} = [P(\theta_s)][v_{sabc}] \; ; \begin{bmatrix} i_{sd} \\ i_{sq} \end{bmatrix} = [P(\theta_s)][i_{sabc}] \; ; \begin{bmatrix} \psi_{sd} \\ \psi_{sq} \end{bmatrix} = [P(\theta_s)][\psi_{sabc}] \quad \text{(II.13)}$$

$$\begin{bmatrix} v_{rd} \\ v_{rq} \end{bmatrix} = [P(\theta_s)][v_{rabc}] \; ; \begin{bmatrix} i_{rd} \\ i_{rq} \end{bmatrix} = [P(\theta_s)][i_{rabc}] \; ; \begin{bmatrix} \psi_{rd} \\ \psi_{rq} \end{bmatrix} = [P(\theta_s)][\psi_{rabc}] \quad \text{(II.14)}$$

So, the voltage equations can be written as the following:

$$\begin{cases} v_{sd} = R_s i_{sd} + \frac{d\psi_{sd}}{dt} - \omega_s \psi_{sq} \\ v_{sq} = R_s i_{sq} + \frac{d\psi_{sq}}{dt} + \omega_s \psi_{sd} \\ v_{rd} = R_r i_{rd} + \frac{d\psi_{rd}}{dt} - (\omega_s - p\omega_r)\psi_{rq} \\ v_{rq} = R_r i_{rq} + \frac{d\psi_{rq}}{dt} + (\omega_s - p\omega_r)\psi_{rd} \end{cases} \quad \text{(II.15)}$$

where:

$$\omega_s = \frac{d\theta_s}{dt} \; ; \omega_r = \frac{d\theta_r}{dt} \quad \text{(II.16)}$$

The flux equations can be written as the following:

$$\begin{cases} \psi_{sdq} = L_s[i_{sdq}] + M_{sr}[i_{rdq}] \\ \psi_{rdq} = L_r[i_{rdq}] + M_{sr}[i_{sdq}] \end{cases} \quad \text{(II.17)}$$

II.2.5.2 Mechanical equations

The rotor motion is followed by the dynamic equation as

$$J\frac{d\omega_r}{dt} = T_e - T_L - f\omega_r \quad \text{(II.18)}$$

The electromagnetic torque is given by:

$$T_e = p\frac{M_{sr}}{L_r}(\psi_{rd} i_{sq} - \psi_{rq} i_{sd}) \quad \text{(II.19)}$$

or, in another expression:

$$T_e = p(\psi_{sd} i_{sq} - \psi_{sq} i_{sd}) \quad \text{(II.20)}$$

As well-known in the literature, the model of the induction machine expressed in the rotating frame (*d, q*) is often used for the field-oriented control design.

II.3 Voltage Source Inverter (VSI)

An inverter is a static converter ensuring DC to AC conversion. it periodically changes the connections between the input and the output to obtain alternating voltage and current at the output [37]. The schematic of the two-level voltage source inverter is presented in Figure II.5, as shown, the inverter is supplied by a DC link voltage Vdc which is provided by a rectifier or another DC source, The converter consists of the three legs with IGBT transistors with parallel free-wheeling diodes in the most applications [5], [6].

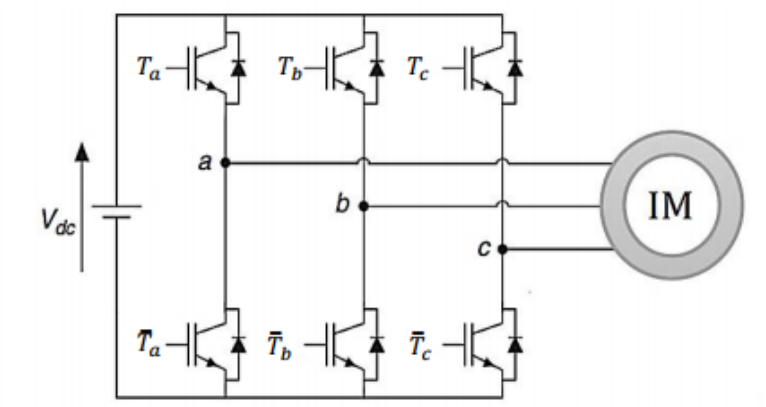

Figure II.5. *Three-phase voltage inverter* [6].

To avoid a short-circuit of the source, it is necessary to respect the following states as:

$S_i = 1$, T_i is ON and $\overline{T_i}$ is OFF.

$S_i = 0$, T_i is OFF and $\overline{T_i}$ is ON.

with: i= a, b, c.

The output voltages inverter depend on switching states by the following matrix [38]:

$$\begin{bmatrix} V_A \\ V_B \\ V_C \end{bmatrix} = \frac{V_{dc}}{3} \begin{bmatrix} 2 & -1 & -1 \\ -1 & 2 & -1 \\ -1 & -1 & 2 \end{bmatrix} \begin{bmatrix} S_a \\ S_b \\ S_c \end{bmatrix} \quad \text{(II.21)}$$

The voltage vector is generated by the following equation [6]:

$$V_s = \sqrt{\frac{2}{3}} V_{dc} \left[S_a + S_b e^{-j\frac{2\pi}{3}} + S_c e^{-j\frac{4\pi}{3}} \right] \quad \text{(II.22)}$$

The inverter output voltage constitutes a cyclic and symmetric sequence of vectors [39], There are eight possible positions of the switches states, two states are zero vectors (V_0, V_7) and six states

are active vectors (V_1 to V_6) [5], [6]. The states of the output voltage are represented by space vectors as shown in Figure II.6.

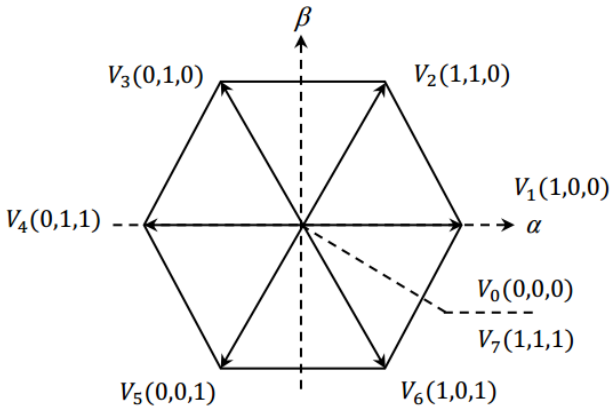

Figure II.6. *The switching states of the output voltage represented by space vectors* [6].

II.4 Pulse Width Modulation (PWM)

The PWM is a technique that allows obtaining the appropriate amplitude and a frequency at the VSI output. Yet, this technique can eliminate harmonics and minimize switching losses [4]. There are many possible PWM techniques proposed in the literature.

The classification of common PWM techniques can be given as [40]:

- Sinusoidal PWM (SPWM)
- Selected harmonic elimination (SHE) PWM
- Minimum ripple current PWM
- Space vector PWM (SVM)

The SVM technique is one of the most popular PWM techniques due to the higher voltage it can produce, easy to realize. Nowadays, the SVM technique is commonly used in several three-phase inverters uses that why it is because it can produce a higher output voltage more than SPWM, and provides lowers torque ripple, and less harmonic of distortion in the current of induction motors, and lower switching losses [4], [41].

II.4.1 Space Vector Pulse Width Modulation

A three-phase two-level inverter provides eight possible switching states that are corresponding to the eight output voltage vectors, V_0 to V_7, as shown in Table II.1. The six of these vectors V_1 to V_6 be called active voltage vectors, their magnitudes are equal to $\frac{2}{3}V_{dc}$. The two other vectors V_0, V_7 are called zero (non-active) voltage vectors where their magnitudes equal to zero. The zero vectors are superfluous but they are used to minimize the switching frequency. When the space

active vectors joined together made a hexagon. This last one consists of six sectors stretching (along) over 360 degrees, for each sector 60 degrees [42]. The space vectors are shown graphically in Figure II.7.

Switch States			**Phase Voltage**			**Space Voltage Vector**
S_a	S_b	S_c	V_{as}	V_{bs}	V_{cs}	$V_n(n=0-7)$
0	0	0	0	0	0	$V_0 = 0\angle 0°$
1	0	0	$\frac{2}{3}V_{dc}$	$-\frac{1}{3}V_{dc}$	$-\frac{1}{3}V_{dc}$	$V_1 = \frac{2}{3}V_{dc}\angle 0°$
1	1	0	$\frac{1}{3}V_{dc}$	$\frac{1}{3}V_{dc}$	$-\frac{2}{3}V_{dc}$	$V_2 = \frac{2}{3}V_{dc}\angle 60°$
0	1	0	$-\frac{1}{3}V_{dc}$	$\frac{2}{3}V_{dc}$	$-\frac{1}{3}V_{dc}$	$V_3 = \frac{2}{3}V_{dc}\angle 120°$
0	1	1	$-\frac{2}{3}V_{dc}$	$\frac{1}{3}V_{dc}$	$\frac{1}{3}V_{dc}$	$V_4 = \frac{2}{3}V_{dc}\angle 180°$
0	0	1	$-\frac{1}{3}V_{dc}$	$-\frac{1}{3}V_{dc}$	$\frac{2}{3}V_{dc}$	$V_5 = \frac{2}{3}V_{dc}\angle 240°$
1	0	1	$\frac{1}{3}V_{dc}$	$-\frac{2}{3}V_{dc}$	$\frac{1}{3}V_{dc}$	$V_6 = \frac{2}{3}V_{dc}\angle 300°$
1	1	1	0	0	0	$V_7 = 0\angle 0°$

Table II.1. *Output voltage vectors corresponding to the switching states* [41].

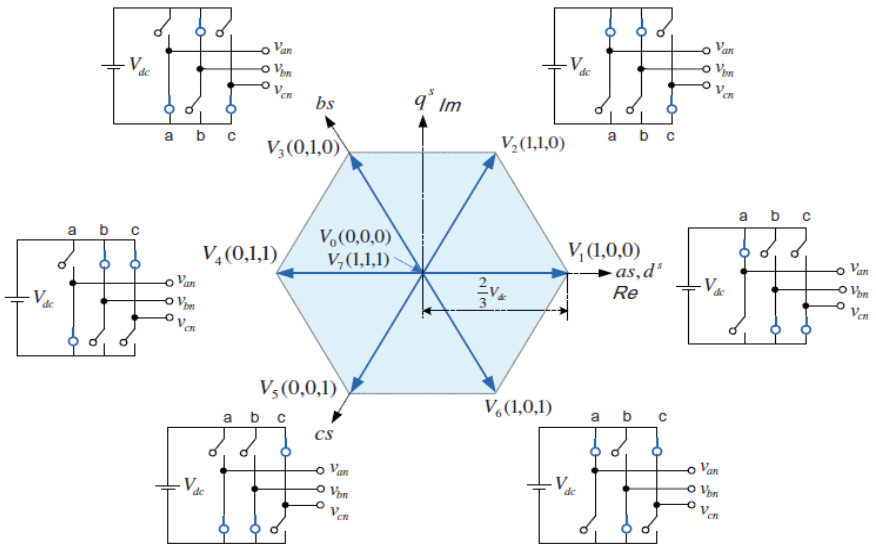

Figure II.7. *Vectors of Output Voltage in the complex plane (d-q axes)* [4].

In the SVPWM technique, it can produce a reference voltage of the output inverter by using the two active voltages neighbors to V_s^* and the zero vectors from the eight voltage vectors. This technique has the same fundamental volt-second average as given the voltage reference vector V_s^* along the modulation (switching) period T_s. In the linear modulation range, the voltage reference follows the circular trajectory. This last one will be a hexagon boundary when the inverter is operating in the six-step mode [4].

In the SVPWM technique, the maximum value of the reference vector amplitude that can be approximated is equal to the radius of the circle that can be inscribed within the hexagon. Thus, the maximum obtainable fundamental output voltage is calculated from the right-angled triangle (Figure II.8) as:

$$V_{max} = \left(\frac{2}{3}\right) V_{dc} \cos\left(\frac{\pi}{6}\right) = \frac{1}{\sqrt{3}} V_{dc} = 0.577 V_{dc} \qquad (\text{II.23})$$

Therefore, Modulation Index MI at this condition can be derived as:

$$MI = \frac{V_{max}}{V_{1sw}} = \frac{0.577 V_{dc}}{\frac{2}{\pi} V_{dc}} = 0.907 \qquad (\text{II.24})$$

V_{max}: Maximum phase voltage,

V_{1sw}: Fundamental peak value ($\frac{2}{\pi} V_{dc}$) of the square-phase voltage wave.

This means that the maximum value of the peak voltage can be obtained from the SVPWM technique corresponds to 90.7% of the output voltage in the square wave operation. In the sinusoidal PWM (SPWM) technique, the maximum value output voltage is $\frac{V_{dc}}{2}$, when using SVPWM is $(2V_{dc}/3)/(V_{dc}/2) = 1.154$. The SVPWM method is 15.47% higher than the SPWM method. Therefore, the dc-link utilization of the two-level inverter is better in the SVPWM method compared to the SPWM [40], [41], [43].

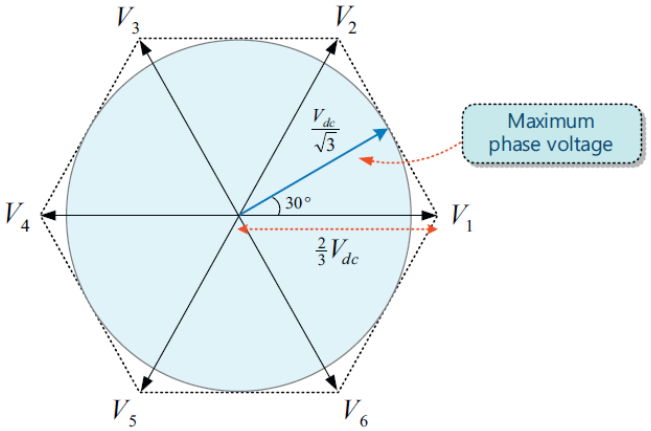

Figure II.8. *The possible range of the voltage reference vector in the SVM* [4].

The first step in SVPWM implementation is the determination of the duration time of each voltage vector. When the reference voltage in sector 1 is, the first vector V_1 is applied during time T_1 and the other vector V_2 is applied during time T_2, then one of the zero vectors, V_0 or V_7, is applied during time T_0, where the time of application zero vector T_0 is remaining time over T_s period, $T_0 = T_s - T_1 - T_2$. Through these steps, it is possible to generate the reference output voltage vector over the modulation period T_s. Hence, using the equal volt-second principle, for sector 1:

$$V_s^* T_s = V_1 T_1 + V_2 T_2 + V_0 T_0 \quad (\text{II.25})$$

As an example, in the first sector 1 ($0 \leq \theta \leq \frac{\pi}{3}$), Equation (II.25) can be decomposed into two components the real and imaginary as:

$$\begin{cases} |V_s^*| \cos(\theta)\, T_s = \frac{2}{3} V_{dc} T_1 + \frac{2}{3} V_{dc} \cos\left(\frac{\pi}{3}\right) T_2 \\ |V_s^*| \sin(\theta)\, T_s = \frac{2}{3} V_{dc} \sin\left(\frac{\pi}{3}\right) T_2 \end{cases} \quad (\text{II.26})$$

Solving equations (II.26) for the duration times T_1 and T_2:

$$T_1 = \frac{\sqrt{3}|V_s^*|}{V_{dc}} \sin\left(\frac{\pi}{3} - \theta\right) T_s \quad (\text{II.27})$$

$$T_2 = \frac{\sqrt{3}|V_s^*|}{V_{dc}} \sin(\theta)\, T_s \quad (\text{II.28})$$

$$T_0 = T_s - T_1 - T_2 \quad (\text{II.29})$$

Figure II.9 shows the generation of the voltage reference process in the first sector.

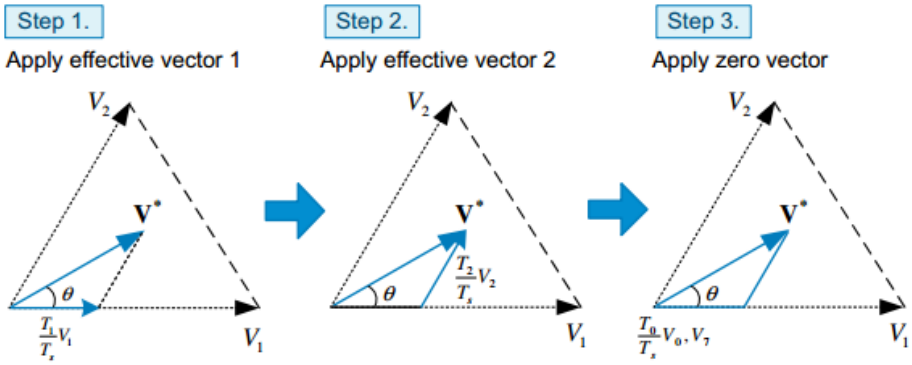

Figure II.9. *The process of generating the reference voltage vector in the first sector* [4].

The calculation times for the reference voltage vector in all sectors give the following, where $k = 1, 2, \ldots 6$ is the sector number:

$$T_1 = \frac{\sqrt{3}|V_s^*|}{V_{dc}} \sin\left(k\frac{\pi}{3} - \theta\right) T_s \quad (\text{II.30})$$

$$T_2 = \frac{\sqrt{3}|V_s^*|}{V_{dc}} \sin\left(\theta - (k-1)\frac{\pi}{3}\right) T_s \quad \text{(II.31)}$$

$$T_0 = T_s - T_1 - T_2 \quad \text{(II.32)}$$

After the duration time of calculation, the next step in SVM implementation is the selection of the switching sequence. To obtain a better harmonic performance and constant switching frequency, each leg should change its state only once in each switching period, which is called the symmetrical SVM technique. In this technique, the total switching time interval T_s is dividing into two parts. The first part begins with the zero vector (000) is applied for 1/4th of the total time T_0, followed by two neighbor active state vectors for their half duration times and then again zero vector (111) is applied for 1/4th of the total time T_0. In the second part, the switching sequence is a mirror image of the first one [4], [41], [43].

As an example in the sector 1, the switching sequence in the first part:

$$V_0(000) \rightarrow V_1(100) \rightarrow V_2(110) \rightarrow V_7(111)$$

In the second part is reversed:

$$V_7(111) \rightarrow V_2(110) \rightarrow V_1(100) \rightarrow V_0(000)$$

The switching pattern for the sector I is showing the voltages leg in one switching period T_s, see Figure II.10.

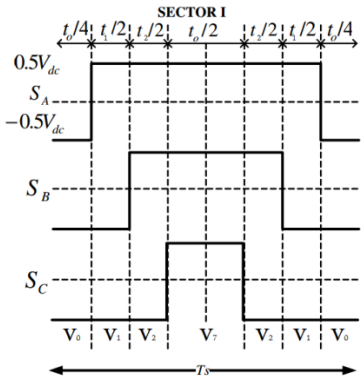

Figure II.10. *Switching sequence of the first sector* [41].

II.5 Conclusion

In this chapter, the mathematical behavior of IM is described in the framework of the bi-phase space vectors (d-q) reference for propose to control and estimate the variables of them. Also, the SVPWM structure and its basic principles have been well discussed. As well-known that the SVPWM (or SVM) technique is commonly used in many applications in industrials thanks to its capability to produce a higher output voltage of 15.5% compared to classical techniques named SPWM. In the next chapters, the SVM strategy will be used as the main part to drive the motor-pump system.

CHAPTER III

DTC-SVM Control for Induction Motor

III.1 Introduction

Over 30 years ago, Takahashi and Depenbrock have invented a control technique for electric motor drives called the Direct Torque Control (DTC) [44]. This classical technique is focused to replace the technique of Field-Oriented Control (FOC), but it has some drawbacks such as variable switching frequency, high torque ripple. To improve that, there are several control structures are proposed in the literature, and one of them, a DTC-SVM technique that is characterized by its constant switching frequency and low torque ripple ... etc. In this chapter, a technique of DTC-SVM is described and discussed using it as part of the electric motor drive. All that is verified numerically exploiting the Simulink/MATLAB.

III.2 Direct Torque Control with Space vector modulation

The DTC which incorporates the technique of space vector modulation is a choice to overcome the drawbacks which are inherently included in the classical DTC, this technique of control allows us to reduces the torque and current ripples [45]. As archived in the literature, the DTC-SVM is proposed firstly by Habetler in 1992 [46]. Figure III.1 shows a general block diagram of DTC-SVM.

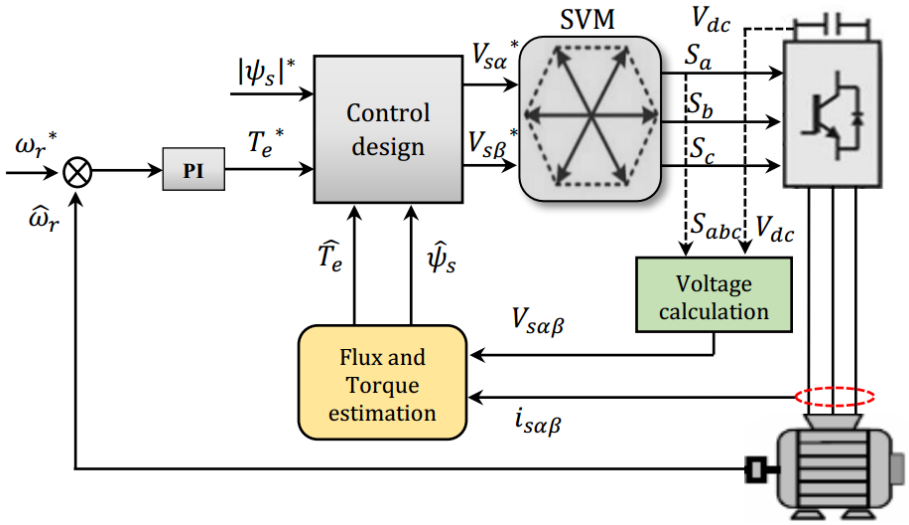

Figure III.1. *General block diagram of SVM direct torque control* [6].

Different structures of DTC-SVM methods are presented in the next section.

III.3 Structures of DTC-SVM

III.3.1 DTC-SVM strategy using closed-loop flux control

The DTC-SVM scheme with a closed flux control is shown in Figure III.2, the principle of operation of this strategy is based on driving the stator flux vector toward the corresponding reference vector defined by the input commands [46].

The d-q components of stator flux are defined as:

$$\psi_{sdc} = \frac{L_s}{L_M}\left(\psi_{rc} + \frac{L_r}{R_r}\sigma\frac{d\psi_{rc}}{dt}\right) \quad \text{(III.1)}$$

$$\psi_{sqc} = \frac{2}{pm_s}\frac{L_r}{M_{sr}}\sigma L_s\frac{T_{ec}}{\psi_{rc}} \quad \text{(III.2)}$$

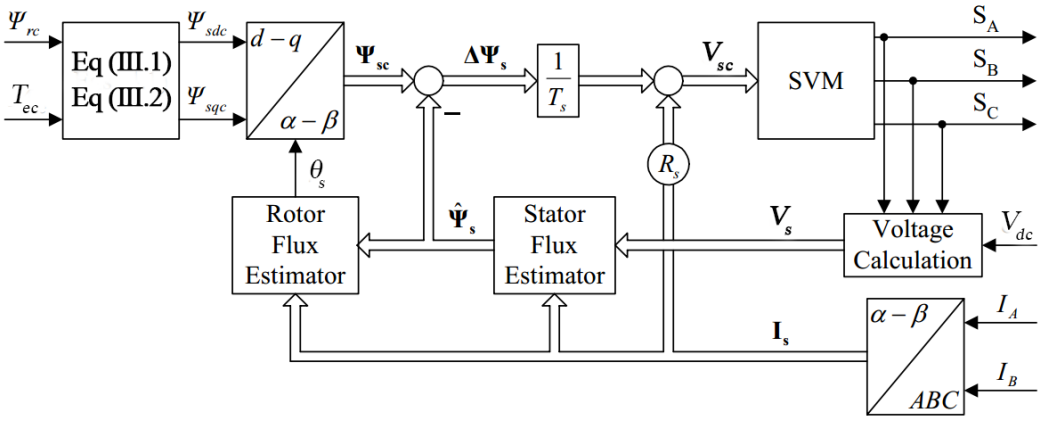

Figure III.2. *DTC-SVM scheme with a closed flux control* [5].

III.3.2 DTC-SVM strategy using closed-loop torque control

The DTC-SVM strategy using closed-loop torque control is mainly based on control of the load angle δ_ψ using the PI controller. Also, the reference stator flux vector should be calculated by knowing the stator flux position and the torque angle as [5], [47]:

$$\psi_{sc} = \psi_{sc}e^{j(\theta_s+\Delta\delta_\psi)} \quad \text{(III.3)}$$

Then, the reference stator flux vector is compared with the estimated value to obtain the flux error $\Delta\psi_s$ which is used to calculate the reference voltage vector V_{sc}. This strategy has a simple structure because it has only one PI controller in which makes the DTC control easier to implement. The block diagram of the DTC-SVM strategy using closed-loop torque control is given in Figure III.3.

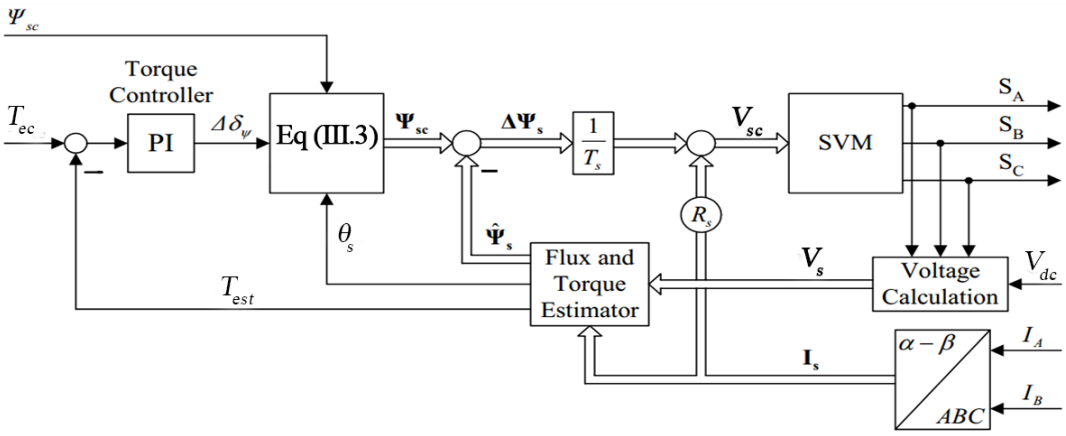

Figure III.3. *DTC-SVM scheme with closed torque control* [5].

III.3.3 DTC-SVM strategy using closed-loop flux and torque control in polar coordinates

This method provides further development when both of the torque and the stator flux magnitude are controlled. As shown in Figure III.4, the stator flux error $\Delta\psi_s$ is calculated through both outputs $\Delta\gamma_s$ and k_ψ of the torque and flux controllers, respectively [38]. As:

$$\Delta\psi_s(k) = \psi_s(k) - \psi_s(k-1) = \left(\left[1 + k_\psi(k)\right]e^{j\Delta\gamma_s(k)} - 1\right)\psi_s(k-1) \quad (\text{III.4})$$

assume that

$$e^{j\Delta\gamma_s(k)} = 1 + j\Delta\gamma_s(k) \quad (\text{III.5})$$

Therefore, the stator flux error can be written as:

$$\Delta\psi_s(k) = \left(\left[k_\psi(k) + j\Delta\gamma_s(k)\right].\psi_s(k-1)\right) \quad (\text{III.6})$$

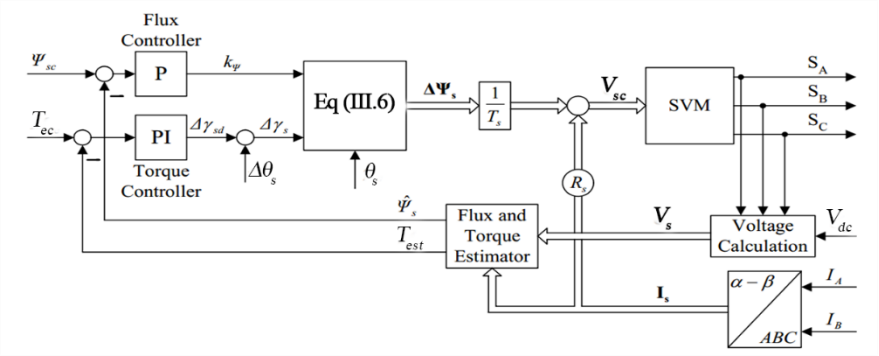

Figure III.4. *DTC-SVM scheme operated in stator flux polar coordinates* [5].

For improvement of the dynamic performance of the torque controller, the increment of angle $\Delta\gamma_s$ is composed of two parts: the static part $\Delta\theta_s$ that is delivered by the feed-forward loop and the dynamic part, $\Delta\gamma_{sd}$ that is generated by the torque controller.

III.3.4 DTC-SVM with closed-loop torque and flux control in stator flux coordinates

The outputs of the PI flux and torque controllers can be considered as the reference stator voltage components V_{sdc} , V_{sqc}. To fed the SVM-inverter, the command references $V_{s\alpha c}$, $V_{s\beta c}$ are used after applying the transformation matrix ($d-q$ to $\alpha-\beta$). The DTC-SVM scheme with closed-loop flux and torque control in stator flux coordinates is presented in Figure III.5 [5], [47].

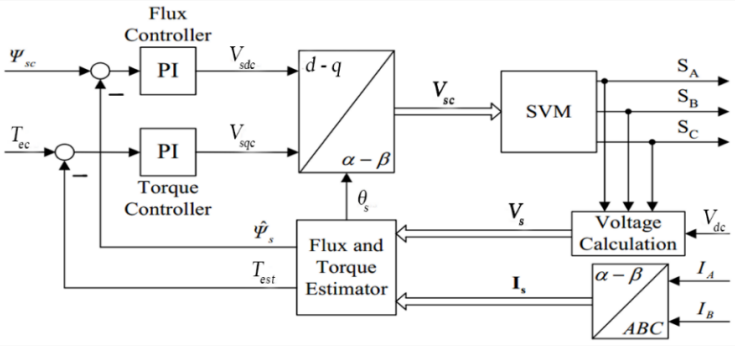

Figure III.5. *DTC-SVM scheme operated in stator flux Cartesian coordinates* [5].

This strategy of direct torque control is selected to validate this project.

III.4 Stator Flux Field-Oriented DTC-SVM

The stator flux oriented direct torque control with space vector modulation depends on the torque and flux closed-loop control in the stator flux coordinate system without any current regulation. The stator flux oriented achieves a decoupling between flux and electromagnetic torque. This method consists of two PI controllers, the first one uses the error between the reference and the estimated values of the flux to produce a reference voltage signal V_{sdc}, where the stator flux vector becomes aligned with the d-axis, the second PI controller uses the error between the reference and the estimated values of the electromagnetic torque to produce a reference voltage signal V_{sqc}, where the torque becomes aligned with the q-axis [49]. Figure III.6 shows the global block diagram of the stator flux oriented DTC with SVM.

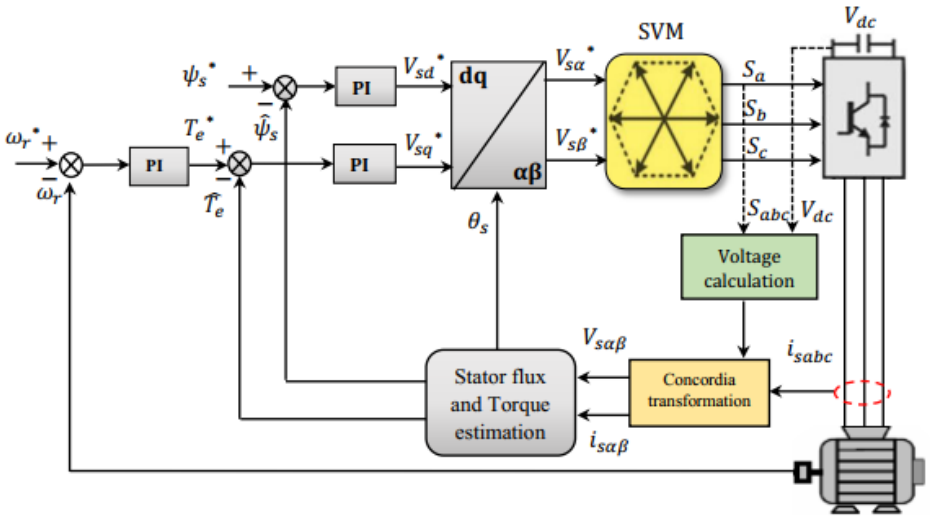

Figure III.6. *The global control scheme of stator flux oriented DTC- SVM* [6].

The stator flux oriented technique depends on the alignment of stator flux with the d-axis, where the stator flux with the q-axis equal to zero, and it can be written as:

$$\begin{cases} \psi_{sd} = \psi_s \\ \psi_{sq} = 0 \end{cases} \quad \text{(III.7)}$$

Consequently, the voltage of the induction motor can be written as:

$$\begin{cases} v_{sd} = R_s i_{sd} + \frac{d\psi_s}{dt} \\ v_{sq} = R_s i_{sq} + \omega_s \psi_s \\ 0 = R_r i_{rd} + \frac{d\psi_{rd}}{dt} - (\omega_s - p\omega_r)\psi_{rq} \\ 0 = R_r i_{rq} + \frac{d\psi_{rq}}{dt} + (\omega_s - p\omega_r)\psi_{rd} \end{cases} \quad \text{(III.8)}$$

Where the flux equation can be described as the following:

$$\begin{cases} \psi_s = L_s i_{sd} + M_{sr} i_{rd} \\ 0 = L_s i_{sq} + M_{sr} i_{rq} \\ \psi_{rd} = L_r i_{rd} + M_{sr} i_{sd} \\ \psi_{rq} = L_r i_{rq} + M_{sr} i_{sq} \end{cases} \quad (III.9)$$

Then the torque and the mechanical equations can be expressed as:

$$T_e = p\psi_s i_{sq} \quad (III.10)$$

$$J\frac{d\omega_r}{dt} = T_e - T_L - f\omega_r \quad (III.11)$$

III.4.1 Flux control design

The input of the flux PI controller is the error between the reference and the estimated values of the flux and its output is a reference voltage signal V_{sdc}.

Based on the motor model equations (III.8-III.9), one has:

$$\left(\frac{R_r}{\sigma L_r} + \frac{d}{dt}\right) V_{sd} = \left[\frac{R_s R_r}{\sigma L_s L_r} + \frac{(R_r L_s + R_s L_r)}{\sigma L_s L_r}\frac{d}{dt} + \left(\frac{d}{dt}\right)^2\right]\psi_s + R_s i_{sq}(\omega_s - p\omega_r) \quad (III.12)$$

with

$$R_s i_{sq}(\omega_s - \omega_r) \approx 0 \quad (III.13)$$

the equation (III.12) becomes as:

$$\left(\frac{R_r}{\sigma L_r} + \frac{d}{dt}\right) V_{sd} = \left[\frac{R_s R_r}{\sigma L_s L_r} + \frac{(R_r L_s + R_s L_r)}{\sigma L_s L_r}\frac{d}{dt} + \left(\frac{d}{dt}\right)^2\right]\psi_s \quad (III.14)$$

Based on equation (III.14) and applying the Laplace transformation, the relationship between the stator flux and stator voltage V_{sd} can be written as:

$$G_{\psi_s}(s) = \frac{\psi_s(s)}{V_{sd}(s)} = \frac{A_\psi + s}{s^2 + B_\psi s + C_\psi} \quad (III.15)$$

where, $A_\psi = \frac{R_r}{\sigma L_r}$ $B_\psi = \frac{R_r L_s + R_s L_r}{\sigma L_s L_r}$ $C_\psi = \frac{R_s R_r}{\sigma L_s L_r}$

The flux control loop is shown in Figure III.7, where $G_{R\psi}(s)$ is a transfer function of the PI controller.

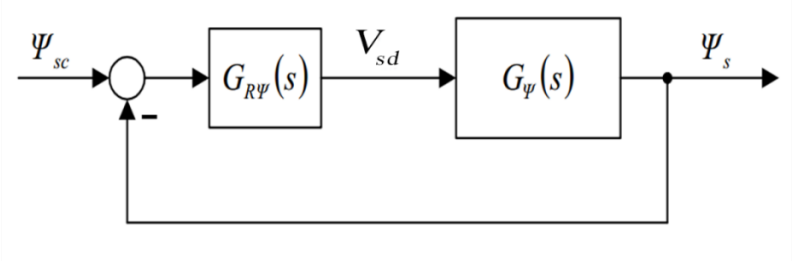

Figure III.7. *The flux control loop.*

There are several methods to tune the gains of the PI controller $K_{p\psi}$ and$K_{i\psi}$, such analysis by Bode diagrams and pole placement. The last one has been used in our work, one has:

$K_{p\psi} = 1647.8$, $K_{i\psi} = 12141.3$.

III.4.2 Torque control design

The input of the PI torque controller is the error between the reference and the estimated values of the electromagnetic torque and its output is a reference voltage signal V_{sqc}.

Based on the motor model equations (III.8-III.9), one has:

$$\left[(R_r L_s + R_s L_r) + \sigma L_s L_r \frac{d}{dt}\right] i_{sq} = L_r V_{sq} - L_r \psi_s p\omega_r + (\omega_s - p\omega_r)\sigma L_s L_r i_{sd} \quad \text{(III.16)}$$

with,

$$(\omega_s - p\omega_r)\sigma L_s L_r i_{sd} \approx 0 \quad \text{(III.17)}$$

If both sides of the equation (III.16) are differentiated, one obtains:

$$\left[(R_r L_s + R_s L_r)\frac{d}{dt} + \sigma L_s L_r \left(\frac{d}{dt}\right)^2\right] i_{sq} = L_r \frac{dV_{sq}}{dt} - L_r \psi_s p \frac{d\omega_r}{dt} \quad \text{(III.18)}$$

Based on equation (III.18) and applying the Laplace transformation, the relationship between the torque and stator voltage V_{sq} is as the following:

$$G_{T_e}(s) = \frac{T_e(s)}{V_{sq}(s)} = \frac{A_T s}{s^2 + B_T s + C_T} \quad \text{(III.19)}$$

where: $A_T = \frac{p\psi_s}{\sigma L_s}$ $B_T = \frac{R_r L_s + R_s L_r}{\sigma L_s L_r}$ $C_T = \frac{p^2 {\psi_s}^2}{\sigma L_s J}$

The torque control loop is shown in Figure III.8, where $G_{RT}(s)$ is a transfer function of the PI controller.

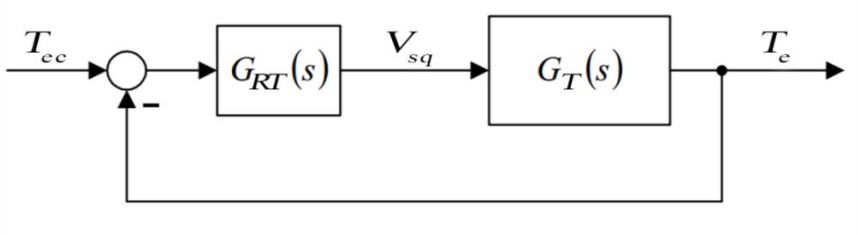

Figure III.8. *The torque control loop.*

The gains of the controller are getting using the same last method, where the gains are obtained as $K_{pT} = 720.5$, $K_{iT} = 1647.8$.

III.4.3 Speed control design

The speed regulation based on the PI controller has generated the reference of electromagnetic torque. The input of this controller is the error between the speed reference and measured speed. The measured speed can be obtained via the speed sensor or estimator.

Using the dynamic equation of an induction motor (III.11), in the transfer function of speed loop is given as:

$$G_{\omega_r}(s) = \frac{\omega_r(s)}{T_e(s) - T_L(s)} = \frac{1}{Js+f} \quad \text{(III.20)}$$

Considering the load torque T_L as a disturbance, the transfer function of the speed control in open loop becomes:

$$G_{\omega_r}(s) = \frac{\omega_r(s)}{T_e(s)} = \frac{1}{Js+f} \quad \text{(III.21)}$$

The speed control loop is shown in Figure III.9, where $G_{RS}\ (s)$ is a transfer function of the PI controller.

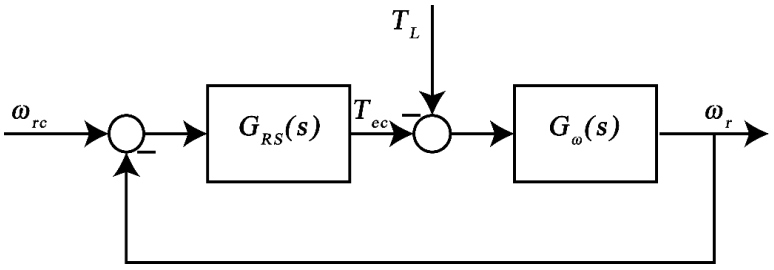

Figure III.9. *The speed control loop.*

The gains of the PI speed controller are obtained as: $K_{ps} = 1.2$, $K_{is} = 24.6$.

III.5 Flux, Torque, and Speed Estimation for Induction Motor Drives

III.5.1 Flux vector estimator

The classical stator flux estimator is based on a voltage model. Such estimator may be directly obtained through the motor model equation as:

$$\hat{\psi}_{s\alpha\beta} = \int \left(V_{s\alpha\beta} - R_s i_{s\alpha\beta}\right) dt \quad \text{(III.22)}$$

$$\hat{\psi}_{s\alpha\beta} = \sqrt{\hat{\psi}_{s\alpha}{}^2 + \hat{\psi}_{s\beta}{}^2} \quad \text{(III.23)}$$

However, in terms of practical implementation, this type of estimator is prone to several sensitivity problems concerning the dc-drift which arise when the pure integrator is used [50]. Therefore, there were several methods proposed to avoid such a problem, one of them, the flux estimator that

was proposed by Lascu and Boldea. The Figure III.11 is presented the flux estimator based on current and voltage models [51].

From the rotor voltages and fluxes (II.15 and II.17) equations, the rotor fluxes can be expressed as:

$$\begin{cases} \psi_{rd} = M_{sr} i_{sd} - \frac{L_r}{R_r}\frac{d\psi_{rd}}{dt} + (\omega_s - \omega_r)\frac{L_r}{R_r}\psi_{rq} \\ \psi_{rq} = M_{sr} i_{sq} - \frac{L_r}{R_r}\frac{d\psi_{rq}}{dt} - (\omega_s - \omega_r)\frac{L_r}{R_r}\psi_{rd} \end{cases} \quad (\text{III.24})$$

The rotor fluxes can be written also as:

$$\begin{cases} \psi_{rd} = \frac{M_{sr}}{1+T_r s} i_{sd} + \frac{1}{1+T_r s}(\omega_s - \omega_r)\psi_{rq} \\ \psi_{rq} = \frac{M_{sr}}{1+T_r s} i_{sq} - \frac{1}{1+T_r s}(\omega_s - \omega_r)\psi_{rd} \end{cases} \quad (\text{III.25})$$

where $T_r = L_r/R_r$ is the rotor time constant.
the d-q rotor flux components are:

$$\begin{cases} \psi_{rd} = \frac{M_{sr}}{1+T_r s} i_{sd} \\ \psi_{rq} = 0 \end{cases} \quad (\text{III.26})$$

the stator flux $\psi^i_{s\alpha\beta}$ calculated in stator coordinates as:

$$\psi^i_{s\alpha\beta} = \frac{M_{sr}}{L_r}\psi^i_{r\alpha\beta} + \frac{L_s L_r - {M_{sr}}^2}{L_r} i_{s\alpha\beta} \quad (\text{III.27})$$

where $\psi^i_{r\alpha\beta}$ is the estimated rotor flux from (III.26) in a stationary reference frame.

The Block diagram of the current model stator flux estimator is shown in Figure III.10.

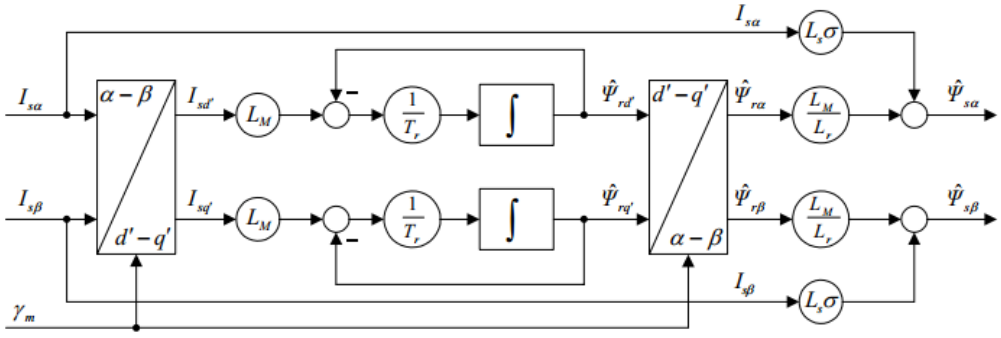

Figure III.10. *Block diagram of the current model flux estimator* [5].

After obtaining $\psi^i_{s\alpha\beta}$ from the open-loop current model, the voltage model is used to estimate the stator fluxes. To correct the value of estimated stator flux should add a compensation term, U_{comp}

regarding the control action of a PI controller, which evaluates the error between the stator fluxes generated by the voltage and current model of the estimator $e_{\psi s\alpha\beta} = (\psi_{s\alpha\beta} - \psi^{i}_{s\alpha\beta})$

$$\psi_{s\alpha\beta} = \frac{1}{s}(V_{s\alpha\beta} - R_s i_{s\alpha\beta} - U_{comp}) \quad \text{(III.28)}$$

$$U_{comp} = (K_p + K_i \frac{1}{s}) e_{\psi s\alpha\beta} \quad \text{(III.29)}$$

The coefficients K_p and K_i may be calculated such that, at zero frequency, the current model stands alone, while at high frequency the voltage model prevails. the PI controller gains are obtained by the following relations

$$K_p = \omega_1 + \omega_2, K_i = \omega_1 \times \omega_2 \quad \text{(III.30)}$$

To achieve a good performance of the flux estimator, the parameters $\omega_1$and ω_2 to be between $2 < \omega_1 < 5$ and $20 < \omega_2 < 30$, respectively [51].

After obtaining the stator flux $\psi_{s\alpha\beta}$, the rotor flux $\psi_{r\alpha\beta}$ is determined as :

$$\psi_{r\alpha\beta} = \frac{L_m}{L_r}\psi_{s\alpha\beta} + \frac{L_s L_r - {L_m}^2}{L_r} i_{s\alpha\beta} \quad \text{(III.31)}$$

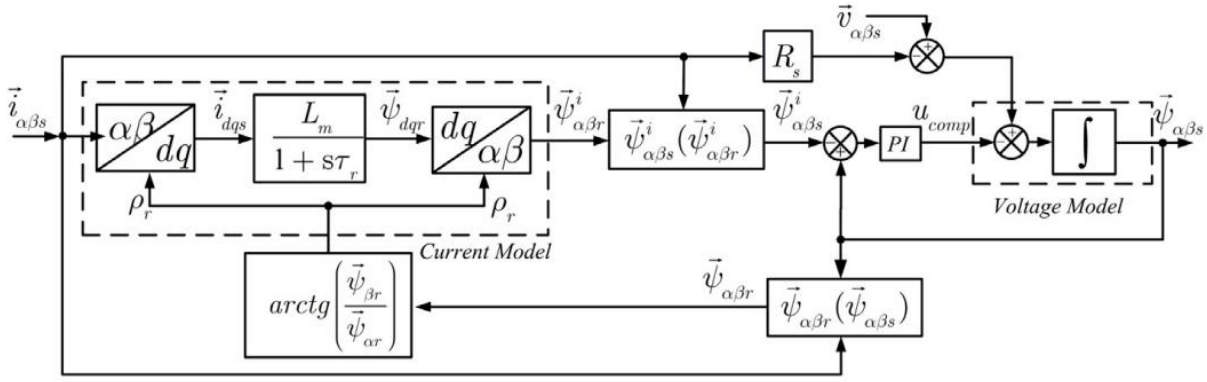

Figure III.11. *Flux estimator based on current and voltage models* [49].

III.5.2 Torque estimation

The estimation torque is depended on the current measurement accuracy and stator flux estimation method as:

$$T_e = \frac{3}{2} p\left(\psi_{s\alpha} i_{s\beta} - \psi_{s\beta} i_{s\alpha}\right) \quad \text{(III.32)}$$

III.5.3 Rotor speed estimation based MRAS

In this project, the Model Reference Adaptive Systems (MRAS) is used to estimate the speed of the induction motor due to its simple structure and robustness. The complete MRAS speed estimator structure can be divided into three components (Figure III.12): Reference model, Adaptive model, and an Adaptive mechanism. The reference model is independent of the speed whereas the adaptive model is dependent to speed. The error vector is generated after comparing the two outputs of the adaptive model and the reference model. This error is processed in the adaptation mechanism to estimate the value of rotor speed. The estimated speed is as feedback to the adaptive model [52].

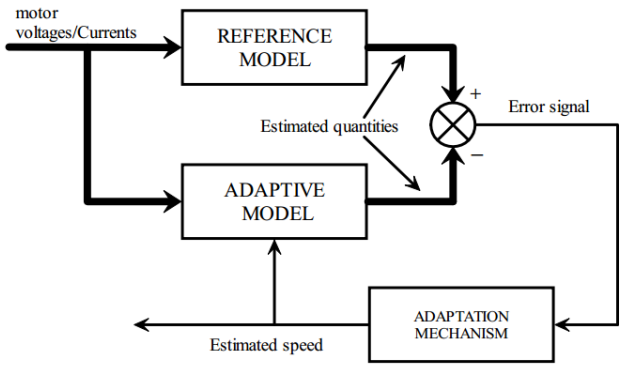

Figure III.12. *Block diagram of speed estimator based on MRAS* [52].

The error between the reference model and the adaptive model can be expressed by:

$$e_{\psi_r} = \hat{\psi}_{r\beta}\psi_{r\alpha}^{\alpha} - \psi_{r\beta}^{\alpha}\hat{\psi}_{r\alpha} \qquad (\text{III.33})$$

In addition, the adaptive model can be written as:

$$\begin{cases} \psi_{r\beta}^{\alpha} = -\frac{1}{T_r}\hat{\psi}_{r\beta} + \frac{L_m}{T_r} i_{s\beta} + \hat{\omega}_r \psi_{r\alpha}^{\alpha} \\ \psi_{r\alpha}^{\alpha} = -\frac{1}{T_r}\hat{\psi}_{r\alpha} + \frac{L_m}{T_r} i_{s\alpha} - \hat{\omega}_r \psi_{r\beta}^{\alpha} \end{cases} \qquad (\text{III.34})$$

where, $\hat{\psi}_{r\alpha}$ and $\hat{\psi}_{r\beta}$ are the rotor fluxes estimated components for the reference model.

$\psi_{r\alpha}^{\alpha}$ *and* $\psi_{r\beta}^{\alpha}$ are the rotor fluxes components for the adaptive model.

The estimated speed is expressed by:

$$\hat{\omega}_r = \left(K_p + K_i \frac{1}{s}\right) e_{\psi_r} \qquad (\text{III.35})$$

III.6 Simulation Results

The DTC-SVM control for three phases 1.5 kW induction motor is implemented using MATLAB/Simulink. The different operating conditions are verified to validate the presented technique, *the discussion of this result is comparing to* ***the classical DTC*** *that is presented at* [6].

- The test at starting up and the steady states:

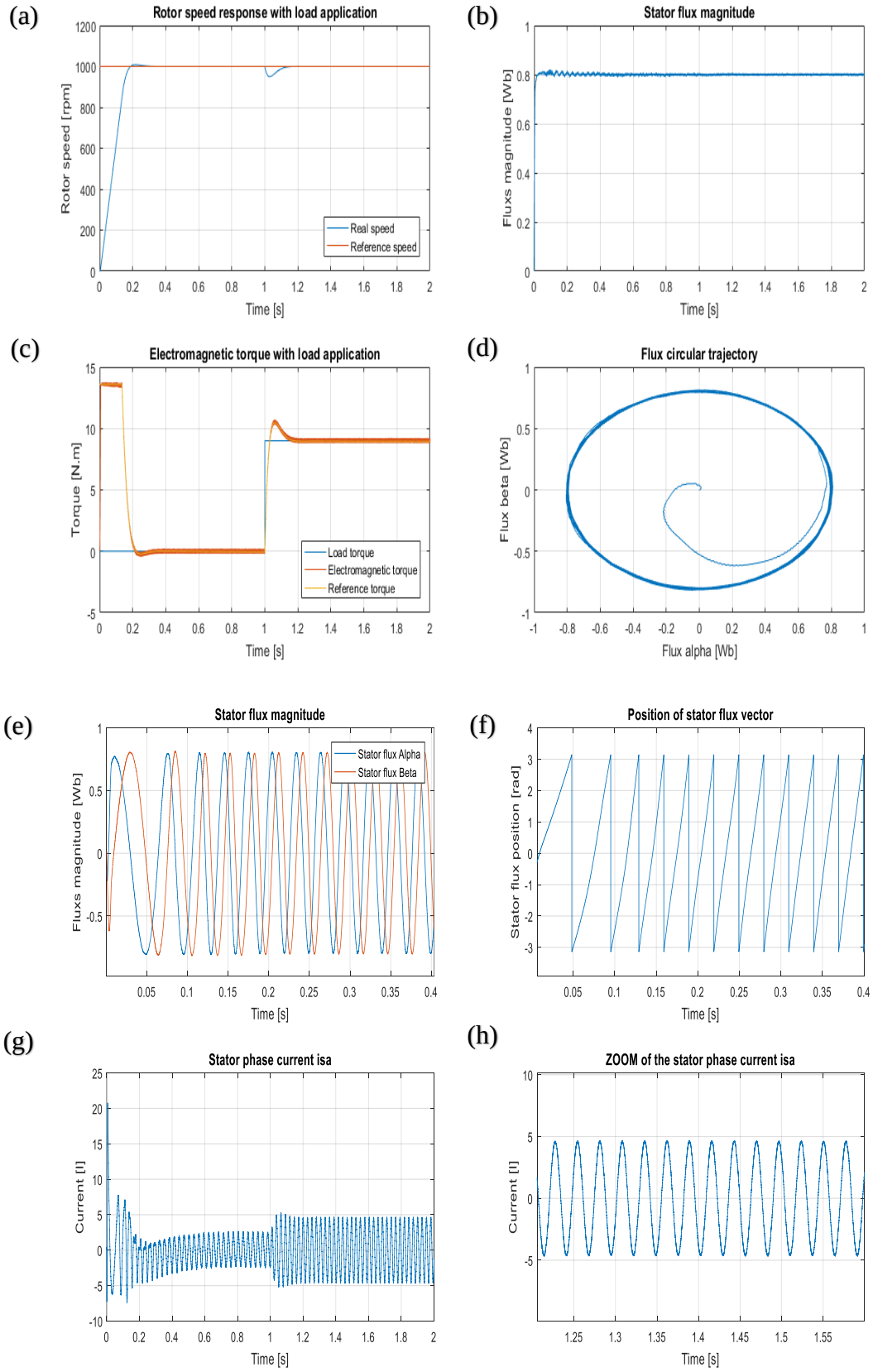

Figure III.13. *Simulation result of starting up and the steady-state case.*

The speed step reference is 1000 rpm with a load torque 9 N.m. Figure III.13 shows the starting up and the steady state's condition, and it shows the rotor speed, torque, stator phase current $i_{s\alpha}$, stator flux components, flux magnitude, and the circular trajectory.

Figure III.13 (a) illustrates the speed responses of DTC- SVM with their reference speed applying the torque load at (t=1s). In the starting up part, the figure shows a fast and good speed response, where its controller loop rejects the torque load in the steady-state part.

Figure III.13 (c) shows the torque response and its reference when inserting the torque load, this response is identical with its reference, where the results of the error equal to zero. It can be noticed easily that has lower ripples compared with classical DTC. Then, in Figure III.13 (g, h) illustrates the stator phase current with its zoom. It shows a smoother sinusoidal current which refers to low harmonics. Next, Figure III.13 (b, d, and e) present the stator flux magnitude, circular trajectory, and components. In these figures, the flux magnitude response is fast at the starting up; the flux components $\psi_{s\alpha}$ *and* $\psi_{s\beta}$ have a good waveform. Therefore, the trajectory has a good circle form and fewer ripples level. Figure III.13 (f) shows the stator flux vector position.

- The test at low and reversing speed:

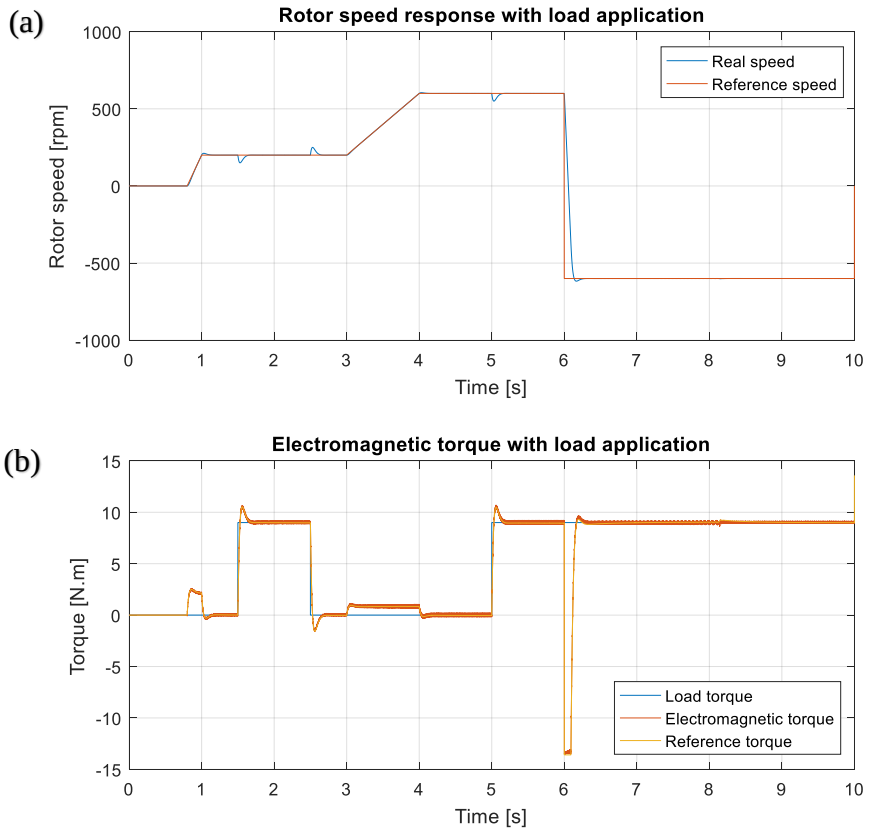

Figure III.14. *Simulation result of low and reversing speed case.*

Figure III.14 (a) presents the test of operating at low and reversing speed response of the studied technique, one shows that the speed value is starting from 200 rpm (1-3 second) to 600 rpm (4-6 second), then applying a reversing speed from 600 rpm to -600 rpm (6 to 10 seconds), one shows the robustness of the presented technique is verified. It can be noticed easily that the speed has an overshoot at the starting up at low-speed region. Also, in the region of reversing speed, and one can be seen that the speed of the motor presents a good fast response. As seen in Figure III.14 (b), the torque response follows its trajectory in a good way, In general, the DTC-SVM technique provides a good dynamic more than the classical DTC.

- Test of MRAS estimator:

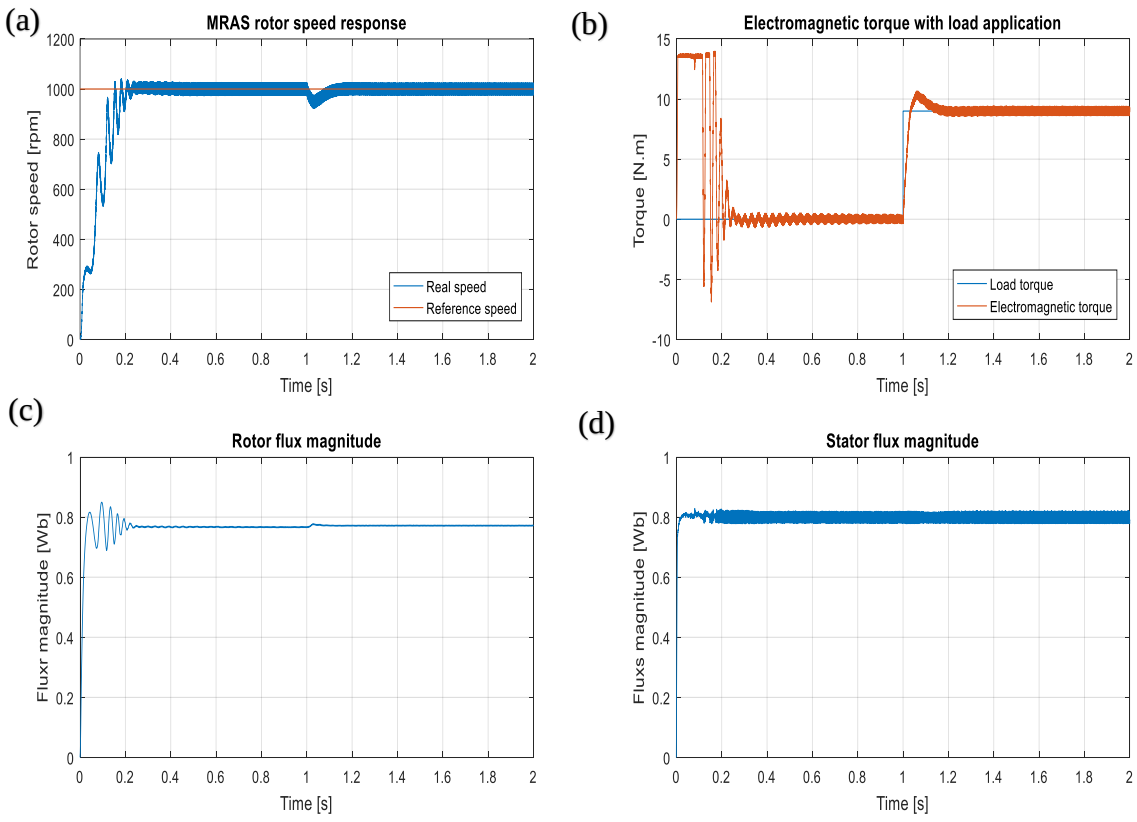

Figure III.15. *Simulation result of DTC-SVM using rotor speed estimation based on MRAS.*

Figure III.15 shows the behavior of IM using a rotor speed estimation based on MRAS. Figure III.15 (a, b, and d) shows the rotor speed, the torque, and the stator flux magnitude, respectively.

III.7 Conclusion

This chapter presents a study of IM behavior using Direct Torque Control with Space Vector Modulation. The DTC-SVM strategy uses three PI controllers for electromagnetic torque, stator flux, and speed control is presented. For better performance of the speed regulation loop, an anti-windup PI controller is used. Then, the MRAS estimator instead of the hardware sensor is presented to minimize the total cost of the system. For more, the DTC-SVM based on the MRAS estimator for IM is numerically studied via the Simulink/Matlab environment.

CHAPTER IV

Photovoltaic Pumping System using DTC-SVM Control for Induction Motor

IV.1 Introduction

In this chapter, we present an overview of the solar photovoltaic water pumping system firstly, then the system design and system control will present and describe, which are the modeling of the pumping system for the design part and the modeling of the P&O algorithm for the control system. Finally, we will simulate the solar water pumping system using Simulink Matlab software, then testing it under different insolation and temperature values to make sure of the effectiveness of this system by discussing the system results.

IV.2 System Description

Solar water pumping systems are very important for many applications. Initially, these systems were pumped using DC motors connected to a pump. However, it was replaced by induction motors due to their better performance, economical and robust. The induction motor is supplied by a photovoltaic (PV) arrays through power converters.

In most of these systems, single-stage and two-stage IM feeding methods were used. In two-stage consisting of a DC-DC converter and a voltage source inverter, the maximum power of the PV panels is usually extracted by maximum power point tracking algorithm (MPPT) using the DC-DC converter. In single-stage, the maximum power point (MPP) of the system is extracted by the VSI converter itself. The induction motor is controlled by DTC-SVM control, where the switching states of the inverter are set by the SVM technique. Figure IV.1 has presented the scheme of the PV array-fed IM drive [3].

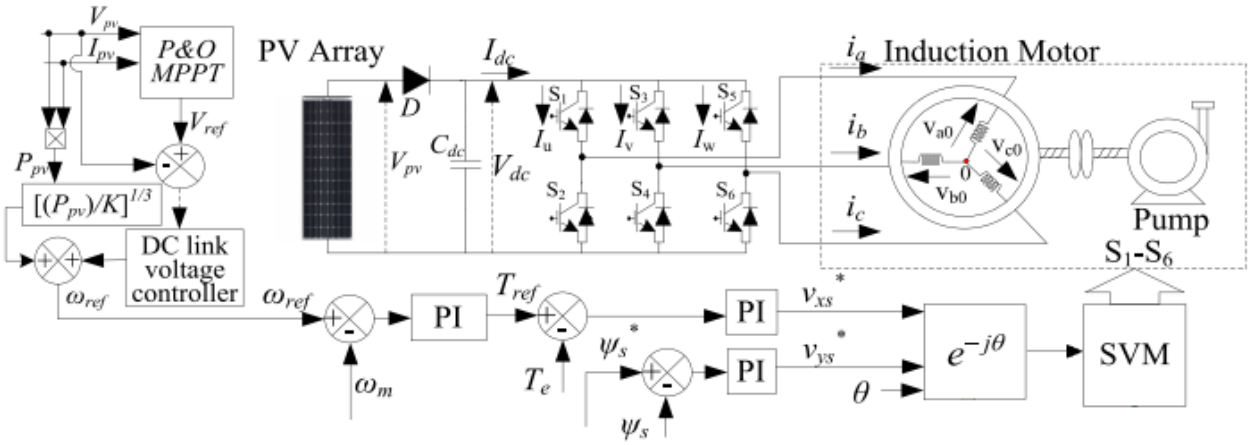

Figure IV.1. *Block diagram of the PV array-fed IM drive* [3].

IV.3 System Design

This design system constitutes a single-stage PV array followed by a VSI fed three-phase induction motor drive operated pump. The PV array operates at maximum power point tracking along with SVM gating logic for effective utilization, the DC-link voltage has been calculated. An Induction motor and voltage source inverter are previously discussed.

IV.3.1 Selection of DC-Link voltage

In order to determine the DC-link voltage of VSI that has to be higher than the peak amplitude voltage, which is given to the motor. It can be estimated as [1]:

$$V_{dc} > V_L\sqrt{2} \quad \text{(IV.1)}$$

where, V_L is a line voltage across the motor terminals.

hence, the value of dc-link voltage is kept V_{dc}.

IV.3.2 DC-link capacitor voltage

The DC-link capacitor can provide sufficient energy at the time of transients, such as a decrease in radiation and an increase in the load [2]. The DC-link capacitor is determined using the following relation:

$$C_{DC-link} = \frac{6aV_pI\,t}{(V_{dc}^2 - V_{dc1}^2)} \quad \text{(IV.2)}$$

where

V_{dc} is the DC-link voltage.

$V_{dc1} = V_L\sqrt{2}$ is the minimum allowable DC-link voltage during the transient condition.

t is the time required to recover the minimum DC-link allowable voltage.

I is the motor phase current, V_p is the phase voltage, $a = 1.2$ is an overloading factor.

IV.3.3 Design of water pump

The most popular pumps are centrifugal pumps and they are used for various applications. These pumps have a nonlinear proportional relationship between the rotor speed and load torque. We can describe them as following [1]:

$$T_p = K_1\omega_r^2 \quad \text{(IV.3)}$$

ω_r is the speed of the induction motor.

where K_1 is proportionality constant of the pump. It can be determined as:

$$K_1 = \frac{T_p}{\omega_r^2} \quad (IV.4)$$

IV.4 System control

The studied system control constitutes two parts: the first one is the MPPT control. It is achieved by three-phase VSI using the P&O algorithm. The second part is motor speed control, which is executed by direct torque control of the drive with the SVM switching scheme.

IV.4.1 Reference speed estimation of induction motor

The reference speed of the induction motor can be estimated by two components. The first one is estimated by the DC-link voltage PI controller. The reference PV voltage is given through MPPT, thus obtained at k^{th} sampling instant, is the DC-link voltage reference V_{dc}^* and it is compared with the PV voltage as follows [1]:

$$V_{dcl(k)} = V_{dc(k)}^* - V_{pv(k)} \quad (IV.5)$$

Figure IV.2 shows the schematic for speed estimation ω_1, the error signal $V_{dcl(k)}$ is fed to the DC link voltage PI controller and the resulting speed error signal at the k^{th} sampling instant and is given as follows:

$$\omega_{1(k)} = \omega_{1(k-1)} + K_{pdc}\left\{V_{dcl(k)} - V_{dcl(k-1)}\right\} + K_{idc}V_{dcl(k)} \quad (IV.6)$$

where K_{pdc} and K_{idc} are the gains of the DC-link voltage PI controller.

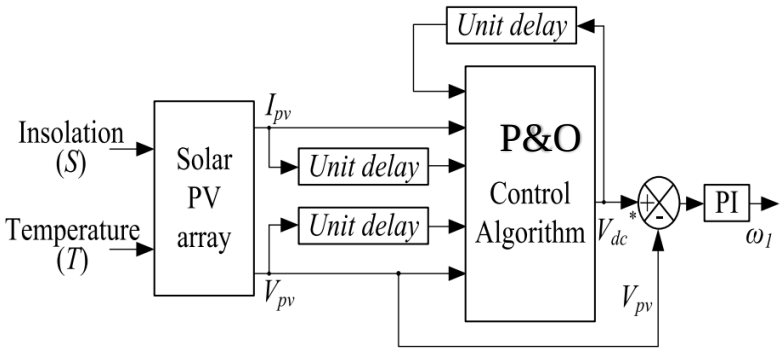

Figure IV.2. *Reference speed generation ω_1 [1].*

Figure IV.3 shows the converted speed term from the PV by the next relation and that gives the second reference speed by affinity law of pump. It can be obtained as:

$$P_{pv} = K_1\omega_2^3 \quad (IV.7)$$

where K_1 is proportionality constant of the pump.

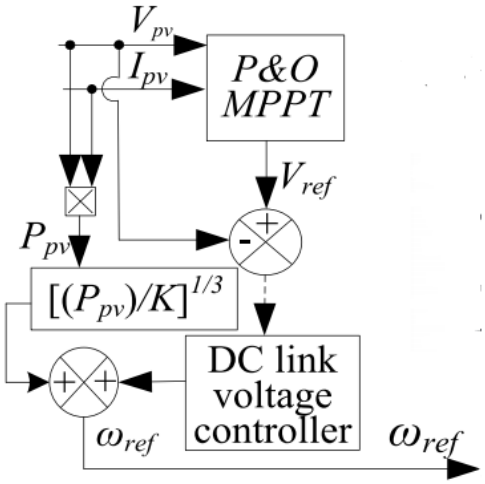

Figure IV.3. *Feedforward speed component* [1].

Hence, the reference speed of the motor is estimated as follows:

$$\omega_{ref} = \omega_1 + \omega_2 \qquad (IV.8)$$

This reference speed is used for control of VSI feeding induction motor drive.

IV.5 Simulation Results

The photovoltaic water pumping system is simulated and modeled in Simulink (MATLAB environment), and the simulation results are shown under conditions of varying the insolation and temperature. The pump load is automatically changed as the rotor speed is varied. Figure IV.4 shows the block simulation of the Photovoltaic Water Pumping System using DTC-SVM control.

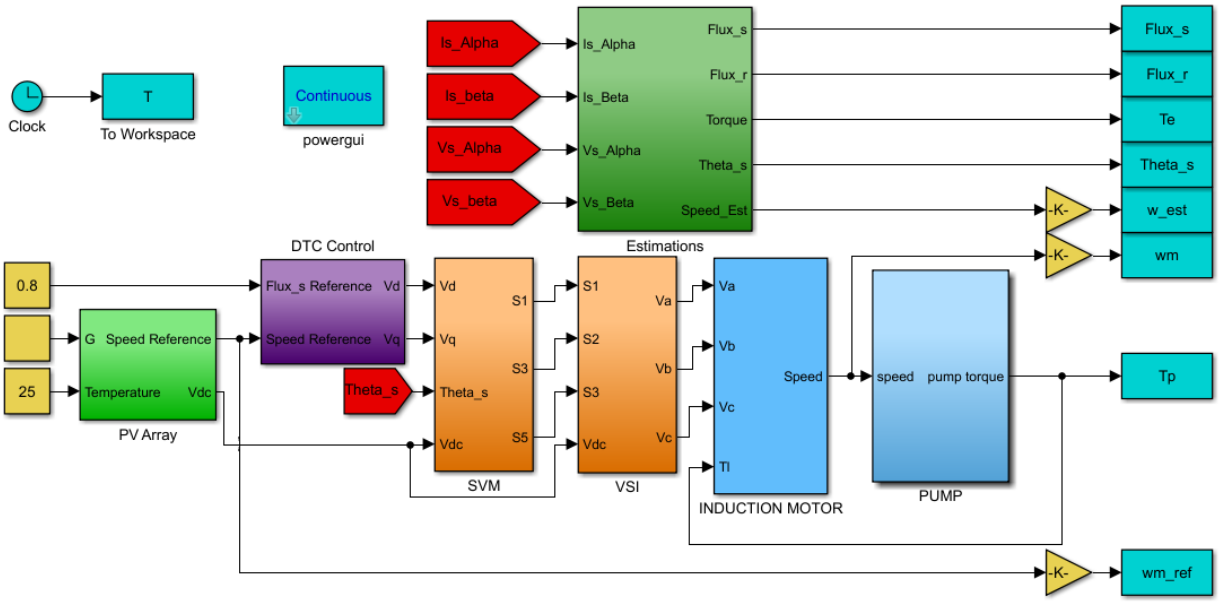

Figure IV.4. *Block simulation of the Photovoltaic Water Pumping System using DTC-SVM control.*

- In the case of the varying in the load pump value by the rotor speed, the result is given as follows:

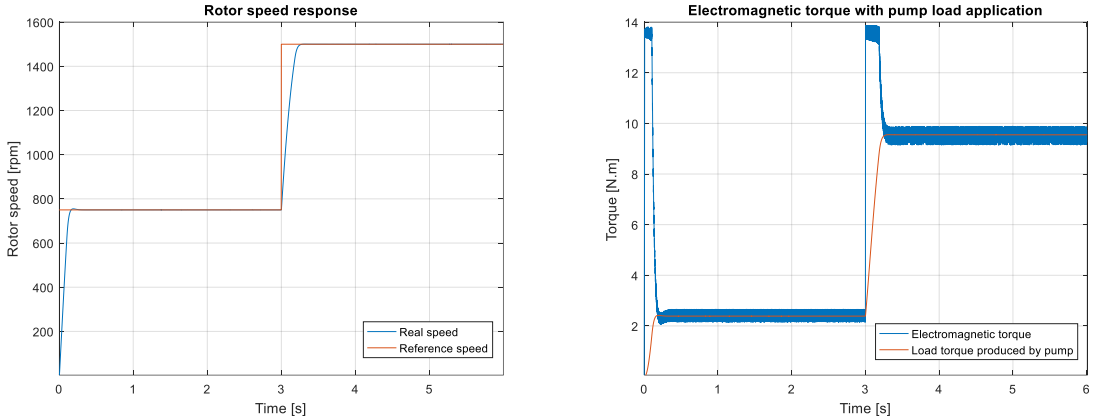

Figure IV.5. *Simulation result of the varying in the load torque produced by the pump.*

Figure IV.5 clearly shows the changing of IM load torque, which is produced by the pump, automatically with the rotation speed. Where the load pump increase when the increase of rotor speed. DTC-SVM can control this load torque of the pump that is applied to the induction motor.

- In the case of the varying in the solar radiation value according to the temperature value, the result is given as follows:

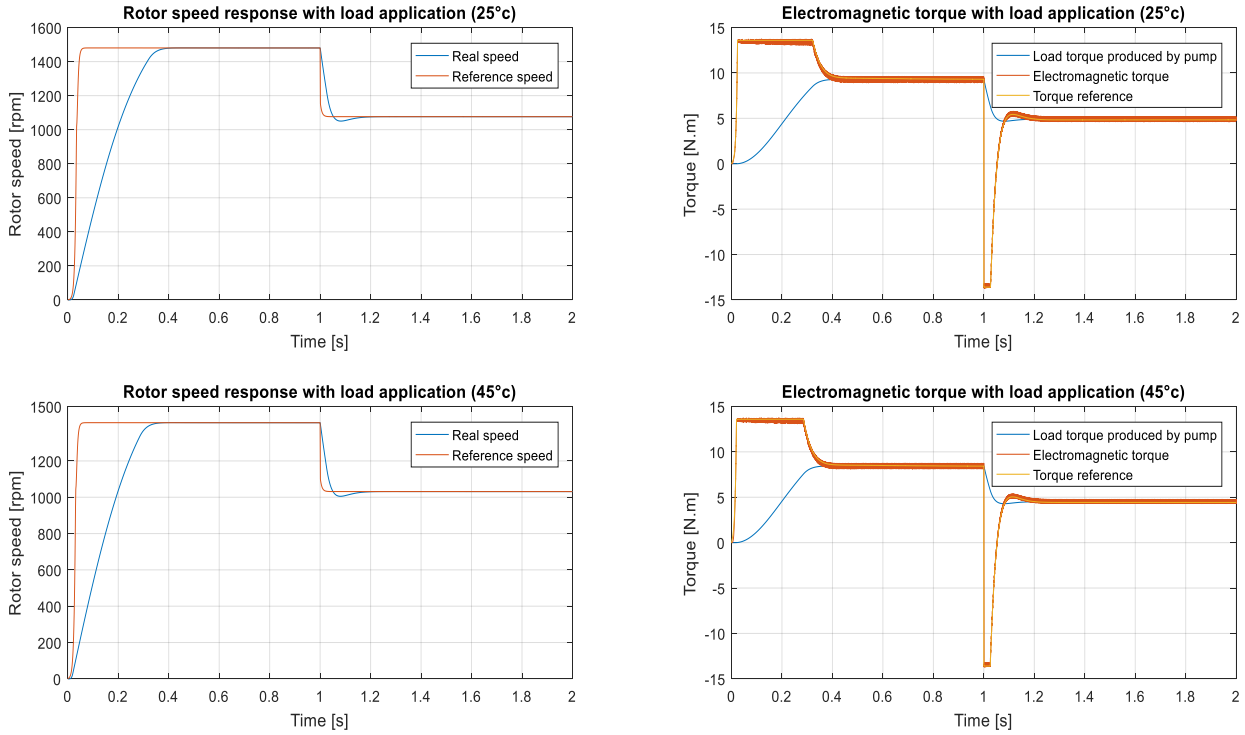

Figure IV.6. *Simulation result of Photovoltaic Water Pumping System using DTC-SVM.*

Figure IV.6 shows rotor speed and electromagnetic torque with a load pump. In the first case, we put the input of the insolation is $1000\ w/m^2$ form (0-1 second) then is $500\ w/m^2$ form (1-2 seconds) with a constant temperature equal to $25\ °c$. In the second one, we put the values of the same interval of the insolation with another constant temperature equal to $45\ °c$.

In the first case, when it is operating at a temperature of $25\ °c$ and insolation $1000\ w/m^2$, which is the ideal part in this case, where it is the ideal case for the system, which is given maximum speed (1480 rpm) and load pump. It can be seen when decreasing the insolation to become $500\ w/m^2$ and the temperature is keeping $25\ °c$, in this case, the speed (1076 rpm) and torque load decrease according to the insolation. In the second case, it can be seen when increasing the temperature to become $45\ °c$ and the insolation is keeping $1000\ w/m^2$, in this part, the speed (1411 rpm) and torque load decrease according to the temperature. Next, it can be seen when keeping the temperature at $45\ °c$ with decreasing the insolation to become $500\ w/m^2$, in this part, the speed (1031 rpm) and torque load decrease according to both the insolation and temperature. Generally, increasing the temperature or decreasing insolation led to decrease in the speed and torque load, which means it affects negatively the efficiency of the PV array.

IV.6 Conclusion

This chapter presents the photovoltaic water pumping system. Firstly, this system is a standalone system that can be described as an induction motor connected to a pump that is fed by a photovoltaic array through a voltage source inverter. Then the modeling of the system design and system control, which are the modeling of the pump and the reference speed estimation MPPT. Secondly, this studied system is simulated in MATLAB/Simulink. Thus, the simulation system shows satisfactory results. These results indicate that the MPPT algorithm can achieve the objective under the variation in the input temperature and solar irradiance. It is clear that the photovoltaic water pumping system is entirely appropriate and suggested in sunny places like South Algeria. Many applications use this system owing to the virtues of simple structure, cost-effectiveness, control, and fairly good efficiency.

GENERAL CONCLUSION

General Conclusion

The work presented in this thesis concerns the modeling and simulation of a photovoltaic pumping system. This system allows supplying the water to isolated sites where no energy source is available. The selected photovoltaic model was simulated in an environment by MATLAB for different temperatures and insolation, the purpose of this simulation is to determine their influence on the system performance, to validate the motor driving efficiency (DTC-SVM), and checking its performance. Where we can conclude depending on our system simulation results some benefices and notices.

Firstly, for selecting the switching states of this system inverter we have used the SVM technique, which provides a constant switching frequency that allows having a reset for the inverter (on/off), it can give a higher voltage value 15% more than SPWM technique. Secondly, the DTC-SVM control is reduced the torque and flux ripples, with a less harmonics of induction motor current that what can give it a good sinusoidal waveform, and give generally a high performance at the starting up and the steady states under the reversing and low speed operating conditions more then the classical DTC. Finally, through the results obtained, the solar water pumping system is stable and gave satisfactory results under different conditions of temperature and insolation, where the electromagnetic torque of the induction motor tracked the load torque that was produced by the pump and controlled by DTC-SVM.

References

[1] S. Shukla and B. Singh, "Single-Stage PV Array Fed Speed Sensorless Vector Control of Induction Motor Drive for Water Pumping," *IEEE Trans. Ind. Appl.*, vol. 54, no. 4, pp. 3575–3585, Jul. 2018, doi: 10.1109/TIA.2018.2810263.

[2] B. Singh, U. Sharma, and S. Kumar, "Standalone Photovoltaic Water Pumping System Using Induction Motor Drive With Reduced Sensors," *IEEE Trans. Ind. Appl.*, vol. 54, no. 4, pp. 3645–3655, Jul. 2018, doi: 10.1109/TIA.2018.2825285.

[3] S. Shukla and B. Singh, "Reduced-Sensor-Based PV Array-Fed Direct Torque Control Induction Motor Drive for Water Pumping," *IEEE Trans. Power Electron.*, vol. 34, no. 6, pp. 5400–5415, Jun. 2019, doi: 10.1109/TPEL.2018.2868509.

[4] K. Sang-Hoon, *Electric Motor Control - DC, AC, and BLDC Motors*, 1st ed. Elsevier, 2017.

[5] M. Żelechowski, "Space Vector Modulated–Direct Torque Controlled (DTC – SVM) Inverter–Fed Induction Motor Drive," Ph.D. thesis, Warsaw University of Technology, 2005.

[6] Abdelkarim Ammar, "Improvement of Direct Torque Control Performances for Asynchronous Machine Using Non-Linear Techniques," Ph.D. thesis, University Mohamed Khider – Biskra, 2017.

[7] "Solar pumping: how renewables will ensure water supply anywhere - BibLus." https://biblus.accasoftware.com/en/solar-pumping-how-renewables-will-ensure-water-supply-anywhere/ (accessed Aug. 24, 2020).

[8] A. H. A. Al-Waeli, H. A. Kazem, M. T. Chaichan, and K. Sopian, *Photovoltaic/thermal (PV/T) systems: Principles, design, and applications*. Springer International Publishing, 2019.

[9] "Heat your water with Solar PV - What about Solar Thermal?" https://nakedsolar.co.uk/solar-pv-solar-thermal/ (accessed Aug. 24, 2020).

[10] F. Vignola, J. Michalsky, and T. Stoffel, *Solar and infrared radiation measurements*. Boca Raton: CRC Press, 2020.

[11] M. Mandalaki and T. Tsoutsos, *Solar Shading Systems: Design, Performance, and Integrated Photovoltaics*, no. D. Springer International Publishing, 2020.

[12] I. Visa, A. Duta, M. Moldovan, B. Burduhos, and M. Neagoe, *Solar Energy Conversion Systems in the Built Environment*. Springer, 2020.

[13] J. Bisquert, *The physics of solar energy conversion*, First edit. {CRC} Press.

[14] A. Goetzberger and V. U.Hoffmann, *Photovoltaic Solar Energy Generation*. Berlin: Springer-Verlag, 2005.

[15] R. Wills, J. A. Milke, S. Royle, and K. Steranka, *Best Practices for Commercial Roof-Mounted Photovoltaic System Installation*. New York, NY: Springer New York, 2015.

[16] Bo Zhao, Caisheng Wang, and Xuesong Zhang, *Grid-Integrated and Standalone Photovoltaic Distributed Generation Systems: Analysis, Design, and Control*. WILEY, 2018.

[17] "Panneaux solaires - future-tech.fr." https://www.future-tech.fr/panneaux-

solaires,fr,8,48.cfm (accessed Sep. 08, 2020).

[18] G. N. Tiwari and S. Dubey, *Fundamentals of Photovoltaic Modules and their Applications*. Royal Society of Chemistry, 2010.

[19] "Connecting Solar Panels Together to Increase Power." https://www.alternative-energy-tutorials.com/energy-articles/connecting-solar-panels-together.html (accessed Aug. 24, 2020).

[20] Suneel Deambi, *Photovoltaic System Design: Procedures, Tools and Applications*, 1st ed. CRC Press, 2016.

[21] S. Sumathi, L. Ashok Kumar, and P. Surekha, *Solar PV and Wind Energy Conversion Systems*. Springer, 2015.

[22] Weidong Xiao, *Photovoltaic Power System Modeling, Design, and Control*. WILEY, 2017.

[23] J. Kenna and B. Gillet, *Solar Water Pumping*. Rugby, Warwickshire, United Kingdom: Practical Action Publishing, 1984.

[24] R. Foster, M. Ghassemi, and A. Cota, *Solar energy: renewable energy and the environment*. Boca Raton FL: CRC Press, 2010.

[25] A. Ivanov-Smolensky, *Electrical machines*, 2nd ed. Moscow: MIR, 1988.

[26] A. Veltman, D. W. J. Pulle, and R. W. De Doncker, *Fundamentals of electrical drives*, vol. 29. Springer, 2007.

[27] Theodore Wildi, *Electrical Machines, Drives, and Power Systems*, 6th ed. 2014.

[28] W. H. Ali, S. I. Abood, and M. N. O. Sadiku, *Fundamentals of Electric Machines: A Primer with MATLAB*, 1st ed. Boca Raton: CRC Press, 2019.

[29] J. J. Cathey, *Electric Machines: Analysis and Design Applying Matlab*. McGraw-Hill, 2001.

[30] T. GÖNEN, *Electrical machines with MATLAB*, 2nd ed. Boca Raton FL: CRC Press, 2012.

[31] R. de Doncker, D. W. J. Pulle, and A. Veltman, *Advanced Electrical Drives: Analysis, Modeling, Control*, vol. 52. Springer, 2011.

[32] "Slip ring Induction Motor, How it works?" https://learnengineering.org/slip-ring-induction-motor-how-it-works.html (accessed Aug. 24, 2020).

[33] A. Masmoudi, *Control Oriented Modelling of AC Electric Machines*. Springer, 2018.

[34] B. Robyns, B. Francois, P. Degobert, and J. P. Hautier, *Vector Control of Induction Machines: Desensitisation and Optimisation Through Fuzzy Logic*, vol. 57. Springer, 2012.

[35] Rachid Abdessemed, *Modélisation et simulation des machines électriques*. ellipses, 2011.

[36] A. Glumineau and J. de L. Morales, *Sensorless AC electric motor control, Robust advanced design techniques and applications*. Springer, 2015.

[37] S. Guy, D. Philippe, and L. Francis, *Electronique de puissance - Structures, commandes, applications*, 10th ed. 5eme rue Laromiguière, Paris: Dunod, 2015.

[38] E. Monmasson, *Power Electronic Converters: PWM Strategies and Current Control Techniques*. Hoboken, NJ 07030: John Wiley and Sons, 2011.

[39] M. P. Kazmierkowski and G. Buja, "Review of Direct Torque Control Methods for Voltage

Source Inverter-Fed Induction Motors," in *IECON Proceedings (Industrial Electronics Conference)*, 2003, vol. 1, pp. 981–991, doi: 10.1109/IECON.2003.1280115.

[40] B. K. Bose, "Modern Power Electronics and AC Drives." Prentice Hall PTR, Upper Saddle River, NJ 07458, 2002.

[41] H. Abu-Rub, A. Iqbal, and J. Guzinski, *High Performance Control of AC Drives with MATLAB/Simulink Models*, 1st ed. John Wiley and Sons, 2012.

[42] M. P. Kazmierkowski, R. Krishnan, F. Blaabjerg, and J. D. Irwin, *Control in Power Electronics: Selected Problems*. Elsevier Science, 2002.

[43] M. F. Rahman and S. K. Dwivedi, *Modeling, Simulation and Control of Electrical Drives*. Institution of Engineering and Technology, 2019.

[44] I. Takahashi and T. Noguchi, "A New Quick-Response and High-Efficiency Control Strategy of an Induction Motor," *IEEE Trans. Ind. Appl.*, vol. IA-22, no. 5, pp. 820–827, 1986, doi: 10.1109/TIA.1986.4504799.

[45] G. S. Buja and M. P. Kazmierkowski, "Direct torque control of PWM inverter-fed AC motors - a survey," *IEEE Trans. Ind. Electron.*, vol. 51, no. 4, pp. 744–757, Aug. 2004, doi: 10.1109/TIE.2004.831717.

[46] T. G. Habetler, F. Profumo, M. Pastorelli, and L. M. Tolbert, "Direct torque control of induction machines using space vector modulation," in *Conference Record of the 1991 IEEE Industry Applications Society Annual Meeting*, 1991, pp. 428–436 vol.1, doi: 10.1109/IAS.1991.178191.

[47] D. Casadei, G. Serra, A. Tani, L. Zarri, and F. Profumo, "Performance analysis of a speed-sensorless induction motor drive based on a constant-switching-frequency DTC scheme," *IEEE Trans. Ind. Appl.*, vol. 39, no. 2, pp. 476–484, Mar. 2003, doi: 10.1109/TIA.2003.808937.

[48] C. Reza, M. D. Islam, and S. Mekhilef, "A review of reliable and energy efficient direct torque controlled induction motor drives," *Renew. Sustain. Energy Rev.*, vol. 37, pp. 919–932, 2014.

[49] B. L. G. Costa, C. L. Graciola, B. A. Angélico, A. Goedtel, M. F. Castoldi, and W. C. de Andrade Pereira, "A practical framework for tuning DTC-SVM drive of three-phase induction motors," *Control Eng. Pract.*, vol. 88, pp. 119–127, 2019.

[50] D. Stojić, M. Milinković, S. Veinović, and I. Klasnić, "Improved Stator Flux Estimator for Speed Sensorless Induction Motor Drives," *IEEE Trans. Power Electron.*, vol. 30, no. 4, pp. 2363–2371, Apr. 2015, doi: 10.1109/TPEL.2014.2328617.

[51] C. Lascu, I. Boldea, and F. Blaabjerg, "A modified direct torque control for induction motor sensorless drive," *IEEE Trans. Ind. Appl.*, vol. 36, no. 1, pp. 122–130, Jan. 2000, doi: 10.1109/28.821806.

[52] B. Kumar, Y. K. Chauhan, and S. P. Singh, "MRAS based speed estimation strategies for induction motor drives: A review," in *2016 7th India International Conference on Power Electronics (IICPE)*, 2016, pp. 1–4.